HHS Public Access

Author manuscript

Cell Chem Biol. Author manuscript; available in PMC 2024 August 17.

Published in final edited form as:

Cell Chem Biol. 2023 August 17; 30(8): 893–905.e7. doi:10.1016/j.chembiol.2023.06.013.

Chemokine Binding to PSGL-1 is Controlled by O-Glycosylation and Tyrosine Sulfation

Christoffer K. Goth[1,2,3,†], **Akul Y. Mehta**[1,†], **Alyssa M. McQuillan**[1], **Kelly J. Baker**[1], **Melinda S. Hanes**[1,4], **Simon S. Park**[1], **Kathrin Stavenhagen**[1,5], **Gertrud M. Hjortø**[2], **Jamie Heimburg-Molinaro**[1], **Elliot L. Chaikof**[1], **Mette M. Rosenkilde**[2], **Richard D. Cummings**[1,*]

[1] Department of Surgery Beth Israel Deaconess Medical Center, National Center for Functional Glycomics, Harvard Medical School, Boston, MA, 02215, U.S.A.

[2] Laboratory for Molecular Pharmacology, Department of Biomedical Sciences, Faculty of Health and Medical Sciences, University of Copenhagen, Copenhagen, Denmark

[3] Current: GLX Analytix ApS, Copenhagen, Denmark

[4] Current: Visterra Inc. 275 2nd Avenue, Waltham, MA 02451, U.S.A.

[5] Current: AstraZeneca, Gothenburg, Sweden

Summary

Protein glycosylation influences cellular recognition and regulates protein interactions, but how glycosylation functions alongside other common post-translational modifications (PTMs), like tyrosine sulfation (sTyr), is unclear. We produced a library of 53 chemoenzymatically synthesized glycosulfopeptides representing N-terminal domains of human and murine P-selectin glycoprotein ligand-1 (PSGL-1), varying in sTyr and O-glycosylation (structure and site). Using these, we identified key roles of PSGL-1 O-glycosylation and sTyr in controlling interactions with specific chemokines. Results demonstrate that sTyr positively affects CCL19 and CCL21 binding to PSGL-1 N-terminus, whereas O-glycan branching and sialylation reduced binding. For murine PSGL-1, interference between PTMs is greater, attributed to proximity between the two PTMs. Using fluorescence polarization, we found sTyr is a positive determinant for some chemokines. We

[*]Lead Contact – To whom correspondence should be addressed: Richard D. Cummings, Ph.D., Director, National Center for Functional Glycomics, Department of Surgery, Beth Israel Deaconess Medical Center, Harvard Medical School, CLS 11087 – 3 Blackfan Circle, Boston, MA 02115, Tel: 1-617-735-4643, rcummin1@bidmc.harvard.edu.

[†]Both authors contributed equally to this work.

Author Contributions

C.K.G. and A.Y.M. devised the synthesis methodology, performed the synthesis, MALDI/HPLC characterization and purification. A.Y.M. performed the printing of the array. C.K.G. performed enzymatic extension of peptides and the fluorescence polarization assay. A.Y.M., C.K.G., A.M.M, and K.J.B. performed the microarray experiments. M.S.H. and S.S.P. developed and synthesized the sulfonate containing peptides and microarray. K.S. performed the MS/MS experiments and analysis. G.M.H. and C.K.G. carried out the chemotaxis experiments. R.D.C. supervised the experiments and guided the project. J.H.M., E.L.C. and M.M.R. provided input and helped with interpreting results and planning experiments. A.Y.M., C.K.G., J.H.M. and R.D.C. wrote the article, and all authors edited and approved the final manuscript.

Declarations of Interest- The authors declare no competing interests.

Inclusion and Diversity- We support inclusive, diverse, and equitable conduct of research.

showed that synthetic sulfopeptides are potent in decreasing chemotaxis of human dendritic cells toward CCL19 and CCL21. Our results provide new research avenues into the interplay of PTMs regulating leukocyte/chemokine interactions.

eTOC Blurb

Using a chemo-enzymatically synthesized library of PSGL-1 N-terminus glycosulfopeptides, Goth et al. identified key roles of these post-translational modifications on interactions between PSGL-1 and chemokines. Using microarray, fluorescence polarization, and chemotaxis assays, they discovered that tyrosine sulfation provides favorable interactions, while complexity of O-glycans negatively affects these interactions.

Graphical Abstract

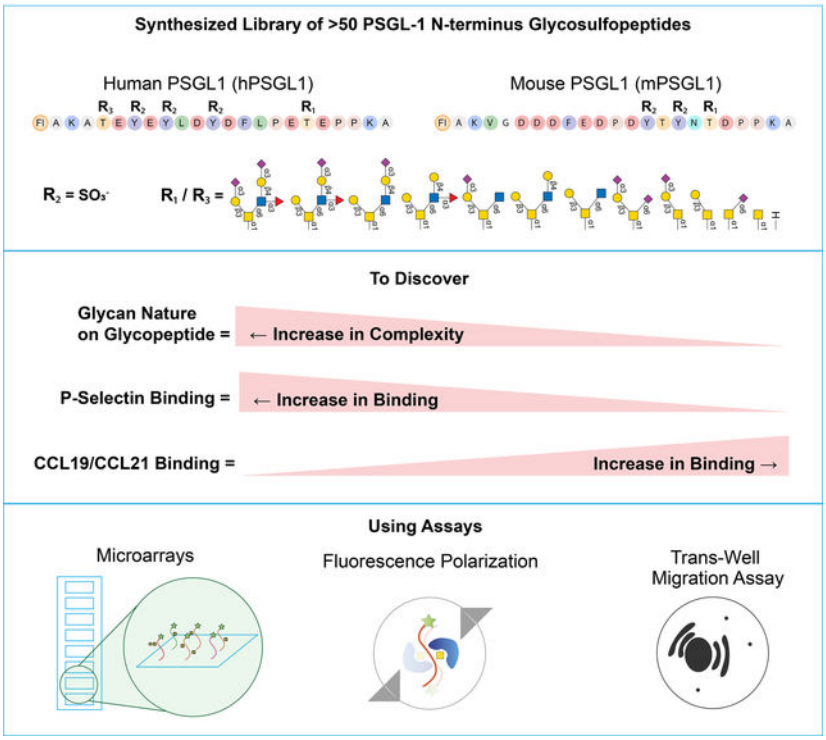

Introduction

P-selectin glycoprotein ligand-1 (PSGL-1) is expressed on the surface of all leukocytes where it facilitates rolling and tethering by functioning as a high-affinity ligand for P-, E- and L-selectin on activated platelets and vascular endothelium [1]. This interaction is crucial in the recruitment of leukocytes in a range of inflammatory responses [2–4] and PSGL-1 holds promise as a target in several diseases [5–7]. PSGL-1 is a transmembrane protein presented as a di-sulfide linked homodimer at the cell surface. A significant proportion of the ectodomain consists of a mucin-like region, which is predicted to be heavily O-glycosylated and may serve to extend the functionally important N-terminus facilitating selectin binding [8]. The N-terminus of PSGL-1 also carries O-glycans [9], more specifically at threonine 57, where the

presence of a sialyl Lewis x determinant Neu5Acα2–3Galβ1–4(Fucα1–3)GlcNAc-R (SLe^x) on a core 2 *O*-glycan is pivotal for its interaction with P-selectin [10]. In addition, tyrosine sulfation of the N-terminus at Tyr46, Tyr48 and Tyr52 is also required for high affinity binding [11], and the relative positioning of sulfotyrosines and O-glycans is critical [12,13].

The known functions for PSGL-1 have expanded beyond selectin binding, as PSGL-1 is an important regulator of several facets of the immune response [14–16]. One of the more recently described functions is the ability of PSGL-1 to bind chemokines, including CCL19, CCL21 and CCL27 [17–19]. Chemokines are a group of small, secreted signaling proteins that direct the trafficking of immune cells in the body through activation of cognate receptors. There are more than 50 chemokines and 25 chemokine receptors (CCRs) which show a high degree of complex and overlapping interactions and binding patterns that are not well understood at the molecular level [20]. The chemokine system is central to homeostasis, development and inflammation, and holds significant potential as a therapeutic target [21].

Sulfotyrosines in the N-termini of several chemokine receptors have been shown to increase affinity for chemokine ligands [22,23]. A recent report demonstrated that sulfated peptides based on the CCR2 N-terminus show potential as a therapeutic [24]. In a few cases, O-glycosylation of CCRs has also been reported to affect chemokine binding and function [25–28]. As we have recently reviewed, all chemokine receptors have potential O-glycosylation and tyrosine sulfation motifs in their N-termini [29]. Recently, ligand binding by the chemoattractant receptor, GPR15, was also shown to be regulated by O-glycosylation and tyrosine sulfation, with opposing effects of the modifications [30]. This suggest a general mechanism for regulating chemokine binding through the interplay of O-glycosylation and tyrosine sulfation [29]. The chemokine binding properties of PSGL-1 may be similarly affected by its glycosylation and sulfation status. Supporting this possibility, PSGL-1-dependent chemokine binding by activated T-cells is diminished compared to naïve T-cells [18], potentially due to up-regulation of C2GlcNAc-1 and synthesis of core 2 O-glycans [18]. Yet, there is a lack of information regarding the impact of specific glycans or sulfates at specific acceptor sites, which is partly due to the paucity of technologies that can site-specifically control these modifications. Chemical biology approaches are needed to understand the interplay of these modifications, as mutagenesis approaches coupled with analytical approaches on recombinant proteins cannot fully replicate such complex repertoires of binding determinants.

O-Glycosylation of Ser/Thr residues in glycoproteins is initiated by up to twenty GalNAc-Ts (GalNAc-Transferases) that generate GalNAcα1-Ser/Thr (Tn antigen). The Tn antigen is normally further elongated by a suite of glycosyltransferases and chaperones resulting in many different glycan structures [31]. O-glycans can be remodeled after internalization and on the cell surface, providing a highly dynamic system [32,33]. Tyrosine sulfation is driven by two sulfotransferases (TPST1/TPST2), each with different specificities and expression patterns [34,35]. No clear consensus sequence for these enzymes has been defined, but most known tyrosine sulfation sites occur in sequences with Glu/Asp clusters. Sulfation may be heterogeneous and there is no evidence of regulated dynamic hydrolysis of sulfotyrosines by human enzymes, but it is known that bacterial sulfatases [11] can hydrolyze sulfotyrosines.

Here, we have exploited a novel method to produce comprehensive glycosulfopeptide libraries using a modified version of the Glyco-SPOT synthesis [36]. As PSGL-1 has overlapping binding epitopes for CCL19 and CCL21, along with the chemokine receptor CCR7 [19], and O-glycosylation of CCR7 impacts ligand binding [26,28,37], we focused on these chemokines. We discovered that chemokine binding by human and murine PSGL-1 is dependent on tyrosine sulfation and that the presence of di-sialyl-Le^x determinants block this binding to human PSGL-1. In the case of murine PSGL-1, less complex sialylated structures also block chemokine binding. Furthermore, we provide evidence that Thr44 in human PSGL-1 can be O-glycosylated and we propose that this site has a similar blocking effect as the mouse PSGL-1 glycosylation site. We also observed that the sulfated PSGL-1 peptide inhibits chemotaxis of human dendritic cells in transwell migration assays. Finally, we expand the known chemokine ligands for PSGL-1 by a fluorescence polarization assay, where we demonstrate that CCL5, CXCL10 and CXCL12 bind with high affinity to PSGL-1 peptides.

Results

A novel approach for glycosulfopeptide synthesis

We developed a modified Glyco-SPOT synthesis protocol to produce a library of glycosulfopeptides based on the human and mouse PSGL-1 N-termini (Figure 1). We designed peptides to span the known tyrosine sulfation and O-glycosylation sites. Furthermore, we added a lysine residue to either C- or N-termini to accommodate bidirectional immobilization in subsequent microarray generation steps. We designed the peptide to include N-terminal fluorescein for visualization, purification and fluorescence polarization assay. To accommodate incorporation of tyrosine sulfation, core 1 and core 2 O-glycans, we modified our previously published Glyco-SPOT method [36]. Important adaptations include extended incubation times and repeat coupling when adding tyrosine sulfation and core 1 and core 2 coupled amino acids. For example, we employed 60 minutes and double coupling for sulfated tyrosine and core 1 amino acids, and triple coupling for core 2 containing peptides, as opposed to 20 minutes for normal amino acids. We previously reported the importance of these extra steps for the glycoamino acids, whereas we used double coupling and extended incubation times for sTyr to improve the yields out of caution, and did not do an extensive study to determine if this was required. For assessing the progress of synthesis, we analyzed samples at intervals in synthesis using biopsies and by MALDI-TOF. We found that the sulfation could only be monitored in negative mode and that the loss of sulfate groups upon ionization was largely unavoidable. Consequently, we also performed HPLC analysis using an ammonium acetate buffer system previously described to be suitable for sulfopeptides [38]. After the synthesis was completed, we performed de-protection of peptide side-chain protecting groups on ice to avoid hydrolysis of tyrosine sulfate. Finally, we added a step of hydrazine addition to remove residual acetyls on core 2 containing peptides after release by sodium bicarbonate (Figure 1). We initially used ammonium acetate to remove protective neopentyl groups, but found that sodium bicarbonate in MeOH was also sufficient for removal. After purification, peptides were enzymatically elongated with recombinant glycosyltransferases ST6GalNAc-1, ST3Gal-1, B1,4-GalT, ST3Gal-4 and FUT6. Using combinations of these enzymes, we generated

12 different glycoforms of sulfated (**14**-**27** and **41**-**53**) and non-sulfated (**1**-**13** and **28**-**40**) peptides based on the N-terminal sequence of human (**1**-**27**) and murine PSGL-1 (**28**-**53**) (Figure 2). In parallel, we synthesized the sulfated and non-sulfated N-terminal sequences of human and murine CCR7 and CCR10 chemokine receptors as controls for chemokine binding (Figure 2).

Thr57 is a well-known glycosylation site in human PSGL-1 due to its crucial role in P-selectin binding, whereas the nearby Thr44 has received less attention with respect to O-glycosylation status and functional importance. However, Thr44 is predicted to be O-glycosylated by the NetOGlyc predictor of O-glycosylation [39]. Thus, glycosylation of Thr44 could occur *in vivo* and be involved in non-selectin interactions by PSGL-1 including chemokine binding. Thr44 is located closer to the sulfated tyrosines at positions 46, 48 and 51 compared to the Thr57 site. This, to some extent, resembles the N-terminal sequence of murine PSGL-1 in relative positions of modifications, where the known O-glycosylation site is at Thr58 and the tyrosine sulfation sites are at positions 56 and 54 (Figure 2). By *in vitro* glycosylation, we were able to glycosylate both sites Thr44 and Thr57 in the human PSGL-1 peptide sequence (Figure S1), and by enzymatic elongation we generated a glycosulfopeptide containing a core 2 SLe^x on both of these sites (2 X SLe^x) (**27**), which were included in the peptide library (Figure 2).

A microarray of PSGL-1 glycosulfopeptides

Using our library of novel PSGL-1 peptides and controls, we generated a glycosulfopeptide microarray to interrogate the functional impact of different glycan structures on CCL19 and CCL21 binding. We also included full-length recombinant PSGL-1 for comparison. Other controls included chemokine receptor peptides (**54**-**61**) and previously published PSGL-1 peptides without fluorescein [6] (see Table S1 for complete list with sequences). We initially validated the array by probing with a number of lectins and with the KPL1 antibody that recognizes the human PSGL-1 N-terminal peptide sequence (Figure S2). The signal for peptide **6** and **8** was considerably lower compared to the other peptides due to poor printing efficiency, which was observed even after re-printing and is potentially caused by internal conformations leading to blocking of the lysines. Next, we probed with P-selectin, which demonstrated that both human and mouse P-selectin exhibit cross-species binding to the sulfated PSGL-1 peptides carrying SLe^x in a calcium-dependent manner (Figure 3). We also observed that P-selectin bound to di-sialyl-Le^x (**26**) as well as to the 2 X SLe^x (**27**) containing peptide where both Thr44 and Thr57 carry the SLe^x structure (Figure 3a). In contrast, E-selectin bound to a broader repertoire of glycosylated peptides and required tyrosine sulfation and the human PSGL-1 sequence for binding (Figure 3b).

Tyrosine sulfation, sialic acids and branched O-glycans regulate CCL19 and CCL21 binding to PSGL-1

CCL19 and CCL21 have been reported to be ligands for PSGL-1 and the binding of CCL19 for CCR7 and PSGL-1 has been shown to overlap [19]. Therefore, we focused on the binding of CCL19 and CCL21 and discovered very similar binding patterns between the two chemokines on the array (Figure 4 and Figure S3). Tyrosine sulfation markedly increased the binding signals, and at 1 μg/ml we did not observe any significant binding to the non-

sulfated peptides, except for CCL21 binding slightly to the non-modified murine PSGL-1 peptide (Figure S3). For the human PSGL-1 sequences, core 1 (T-antigen) structures (**17**) showed the highest relative binding. Interestingly, the presence of sialic acid, as in the di-sialyl-Le^x (**26**) and 2 X SLe^x (**27**) peptides, almost completely abolished the binding of both CCL19 and CCL21, while sialylT (**18**) and di-sialylT (**19**) showed apparent reduced binding (Figure 4). Similarly, sialylation caused remarkable decrease in the recognition of mouse sequences. Simple structures such as di-sialylT (**46**) and sialylated branch core 2 structures (**51**-**53**) blocked the CCL19 and CCL21 binding completely. Both chemokines also bound to sulfated hCCR7 and hCCR10, yet neither bound to the recombinant full length PSGL-1 (**68**). The site-specific modifications and structures of the recombinant PSGL-1 are not known. As shown in Figure 3 and Figure S2, P-selectin and KPL1 antibody showed high binding to the recombinant PSGL-1 confirming the presence of the Thr57 glycosylation and the primary sequence. We observed binding of CCL19 to the recombinant full-length PSGL-1 after it was treated on the array with neuraminidase (Figure S3); these results could reflect that glycosylation and/or sulfation of recombinant PSGL-1 expressed in CHO cells is different than our peptides. Note that the neuraminidase treatment may not completely remove every sialic acid. We observed glycosylation of the mouse sequences to have a stronger effect on chemokine binding, potentially due to closer vicinity to the sulfation sites. To investigate if the recombinant PSGL-1 carries another glycosylation at Thr44, we treated recombinant PSGL-1 with neuraminidase and galactosidase and performed MS^2 analysis. While the glycosidases did not completely digest the terminal glycans, the results indicated that only Thr57 was O-glycosylated in the recombinant PSGL-1, all tyrosine were detected to be sulfated whereas the occupancy status was inconclusive due to the lability of sulfates in the mass spectrometer (Figure S4). We hypothesize that similar to peptides **25** and **27**, the SLe^x modification on Thr57 contributes to the lack of binding of CCL19 and CCL21 to recombinant PSGL-1.

The PSGL-1 glycopeptide analogue GSnP-6 was previously demonstrated to display nanomolar affinity to human P-selectin; the blockade of PSGL-1/P-selectin by this compound holds significant therapeutic potential in the future development of treatment strategies for related diseases [6,7,40]. To test if CCL19 and CCL21 would also bind PSGL-1 glycopeptides with tyrosines substituted with sulfonates, we produced another microarray consisting of sulfated peptides with GalNAc (4GSP1) or SLe^x (4GSP6) and sulfonated peptides named GSnP3–7; with Core2, Core2-Gal, Core2-Gal-SA, Core2-Gal-Fuc, SLe^x and di-sialyl-Le^x. The synthesis of these peptides has been described elsewhere [6]. Both chemokines show clear binding to the two sulfated peptides whereas CCL19 showed no binding to the sulfonated peptides and CCL21 showed limited binding to these peptides (Figure S5). This suggests that, unlike P-selectin, CCL19 and CCL21 binding to PSGL-1 glycopeptides distinctly favors sulfated glycoforms and is not enabled by sulfonates.

PSGL-1 sulfopeptides decrease chemotaxis of human dendritic cells towards CCL19 and CCL21

To directly assess the functionality of these modifications, we tested the ability of the sulfopeptide to block CCL19 and CCL21 binding in a chemotaxis assay. Human dendritic cells were plated in the upper chamber of a transwell 24-well and allowed to migrate

towards 3nM of CCL19 or 5nM of CCL21 in the lower chamber with or without PSGL-1 peptide (**# 1**) or sulfopeptide (**# 14**) co-incubated. After two hours of migration, the PSGL-1 sulfopeptide had significantly decreased the chemotactic index for CCL19 and CCL21 to 42% and 63% respectively of the control (Figure 5). For CCL19, the unmodified peptide decreased the chemotactic index to 71% whereas no significant effect was observed for CCL21. These results further confirm that sulfation of PSGL-1 is important for binding to CCL19 and CCL21.

Fluorescence polarization reveals novel chemokine ligands for PSGL-1

To test other chemokine ligands for interactions with PSGL-1, we utilized the fluorescence polarization assay using the sulfated human PSGL-1 peptide and the unmodified human PSGL-1 peptide and probed binding of 11 different chemokines. This method allows for fast screening using low reaction volumes in solution, without the need for antibodies. We probed the sulfated non-glycosylated peptide as the simplest binding peptide observed to bind in our microarray studies with CCL19 and CCL21. Using fluorescence polarization, we observed strong binding for CCL19, CCL21, CCL5, CCL28, CXCL10 and CXCL12, low binding for CCL2 and CCL14, and no binding for CCL3, CCL4, CCL27 and CXCL8 (Figure 6). Sulfation was observed to markedly increase the affinity for CCL5, similar to CCL19 and CCL21, whereas it had little effect for the other strong binders. Based on this result, we analyzed CCL5 binding on the full array where we confirmed that CCL5 binding to PSGL-1 is dependent on tyrosine sulfation of human PSGL-1 peptide (Figure S3). However, unlike what we observed for CCL19 and CCL21, sialylation and O-glycan size does not block the binding, and di-sialyl Lewis X (di-sialyl-Le^x) (**#26**), 2 X sialyl Lewis X (2 X sLe^X) (**#27**) and recombinant PSGL-1 (**#66**) allowed binding by CCL5. These observations significantly expand the potential chemokine ligands for PSGL-1 and suggest that sulfation of PSGL-1 has differential effects for binding of different chemokines, which could be regulated or dysregulated under certain physiological or pathological conditions.

Discussion

Although chemokine binding by PSGL-1 is largely unexplored at the level of chemical biology, previous studies have shown that PSGL-1 binding of CCL19 and CCL21 is more efficient in resting T-cells compared to activated T-cells [18]. Such studies suggest that this might be due to an increase in O-glycosylation of PSGL-1 on activated T-cells, which is conversely required for proper selectin binding. We report here that O-glycan branching and sialylation status negatively affects both human and murine PSGL-1 binding of CCL19 and CCL21 (Figure 4). However, the extended glycosylation of the mouse PSGL-1 sequence is more effective in blocking the binding, which may be due to its closer proximity to the sulfated tyrosines which is only 2 amino acids, whereas the distance from Thr57 to the first sulfated tyrosine in the human sequence is 6 amino acids (Figure 2). Furthermore, the predicted site of O-glycosylation at Thr44 may also block chemokine binding more efficiently which could also explain why we only observe binding of CCL19 or CCL21 to the recombinant PSGL-1 after removing the sialic acids by neuraminidase treatment (Figure S3). Importantly, CCL5 binding showed different characteristics as tyrosine sulfation of human PSGL-1 is the most important determinant and O-glycosylation blocks this effect

minimally (Figure S3). These results suggest the interesting possibility that P-selectin and CCL19/21 binding can be regulated separately by distinct O-glycosylation sites in the PSGL-1 N-terminus and without affecting CCL5 binding. In this study we synthesized with either no sulfation or sulfation at all available tyrosines, but this is not necessarily the situation *in vivo* as sulfation is often reported to be heterogenous. Consequently, future studies may reveal other effects of specific glycan structures when combined with other sulfation patterns.

By fluorescence polarization assays, we probed additional chemokines and observed that CCL5, CCL28, CXCL10 and CXCL12 could bind to sulfated PSGL-1, whereas CCL3, CCL4, CCL7 and CXCL8 did not bind. Interestingly, these binding patterns mirror the reported patterns of heparan sulfate binding, where CXCL12 and CCL5 were found to bind, and CCL3 and CXCL8 did not bind [41]. It is possible that positively charged residues in CCL5, CXCL10 and CXCL12 drive interactions with anionic sulfate groups in both tyrosine sulfation and heparin sulfate. These differential effects suggest that the sulfation may also regulate the chemokine binding capabilities comparable to what has been shown for CCR3, where distinct tyrosine sulfation sites can direct binding specificity [42]. CCL19, CCL21 [18] and CCL27 [17] have been reported to bind PSGL-1. In these reports, several chemokines did not bind, including CCL5 and CXCL12, which we on the other hand, found to be candidates for binding to PSGL-1. However, in those previous studies CCL5 was probed with immobilized rPSGL-1 with SLe^x modification (and potential Thr44 glycosylation) and CXCL12 binding was probed by chemotaxis assays using murine T-cells from WT and PSGL-1 null mice. Therefore, it is possible that glycosylation and sulfation status differs between these experimental setups and these, together with species differences, may explain the divergence between previous work and some of our observations. Furthermore, glycosylation and sulfation status might be regulated under different physiological and pathological conditions, possibly creating a dynamic system. This clearly illustrates the need for accurately controlling the glycosylation and sulfation on individual residues, to fully understand these interactions, and the biology and therapeutic possibilities in chemokine binding to PSGL-1 and other receptors. Future studies are needed to further dissect how glycan structures and individual sulfation sites impact the binding of individual chemokines.

PSGL-1 was originally described as a P-selectin ligand, but as recent studies have shown, PSGL-1 is also a receptor capable of binding other ligands. Recently, the v-domain immunoglobulin suppressor of T-cell activation (VISTA) was identified as a novel pH-dependent ligand for PSGL-1 [43], and found to be dependent on its tyrosine sulfation, but not the presence of SLe^x on Thr57. VISTA represents yet another important immunoregulatory molecule bound by the N-terminal domain of PSGL-1. The increasing number of interaction partners highlight why complex regulation by two or more different PTMs at multiple acceptor sites have evolved. One should also consider the possibility that Thr44 glycosylation affects VISTA binding, due to its closer proximity to the sulfated tyrosines. Tyrosine sulfation affects many biological functions including: ligand binding [22], proteolytic processing [44] and host-pathogen interactions [45]. As we have previously described, the entire family of CC chemokine receptors, as well as viral derived chemokine receptors and chemokine binding proteins, have patterns of tyrosine sulfation and O-glycosylation in their N-terminal domains crucial for initial chemokine recognition [29]. This overlap between

O-glycosylation and tyrosine sulfation may be a general regulatory mechanism to control binding and specificities. Several other proteins including players in the hemostatic system and in cell-cell adhesion likewise carry these motifs in their binding domains and the functional impact remain unexplored.

Genetic engineering and proteomics has advanced our knowledge of the specificity of individual glycosyltransferases and provided new platforms to express proteins with specific glycans [46–48] and control of individual tyrosine sulfation sites in cells by expanding the genetic code is now possible [49]. However, controlling the complex patterns of multiple PTMs in specific protein sequences as expressed in cells is still beyond our control. This is further complicated by the fact that the TPSTs and multiple glycosyltransferases carry O-glycosylation and have predicted sites of sulfation making indirect effects of genetic engineering of these systems difficult, if not impossible, to predict. Similarly, monitoring the exact sites, structures and occupancies of multiple acceptor sites of two different PTMs are currently out of reach.

The strategy presented here offers a solution to some of these challenges and it is easily applied to all proteins carrying the intriguing multi-motif pattern of O-glycosylation and tyrosine sulfation. The peptides can be used for printing microarrays or fluorescence polarization, but can also act as standards in mass spectrometry [36] and potentially other applications. Here we demonstrate negative regulation of chemokine binding by distinct glycosylation structures, similar to the observations for GPR15 and its ligand GPRL15 [30]. Others have shown that sialic acids on CCR5 and CCR7 are needed for proper chemokine binding [25,26], underlining the complexity of these systems. In addition, polysialylation of CCR7 controls its response to CCL21, but not CCL19 by relieving the auto inhibitory conformation of CCL21 [26]. Therefore, there is growing need for tools to accurately study and dissect the functional consequences of these combinatorial multi-motif modifications and interactions. We envision that the method and workflow shown will allow even more detailed studies in the future, and may also lead to the development of peptide-based drugs targeting subsets of chemokines or other glyco-sulfo-dependent interacting partners for therapeutics or diagnostics.

Limitations

The glycopeptide library described in this study was synthesized *in vitro* and may not fully represent the complete range of glycopeptides found *in vivo*, particularly in terms of the various combinations of post-translational modification (PTM) structures and occupancies. A limitation of using peptides and *in vitro* binding assays is the absence of several complex factors that occur *in vivo*, such as the heterodimerization of chemokines, interaction with other binding partners, and the presentation of PSGL-1 epitopes on cell membranes in a different manner than that of the peptides used in our experiments. For the MS/MS analysis, we could not achieve complete galactosidase treatment and therefore there is still some complex glycopeptides present. There are also peaks for sulfate loss in the LC-MS/MS. For the sulfation, due to the lability of the sulfates in the MALDI, we would always observe at least 1 sulfate loss from the actual total mass of fully sulfated glycopeptides.

STAR METHODS

RESOURCE AVAILABILITY

Lead Contact—Further information and requests for resources and reagents should be directed to and will be fulfilled by the Lead Contact, Dr. Richard D. Cummings (rcummin1@bidmc.harvard.edu).

Materials Availability—Glycosulfopeptides generated in this study are available within reasonable limits of quantity, due to the small scale of synthesis, upon request to the Lead Contact.

Data and Code Availability

- MS/MS data was submitted to PRIDE Database. Accession number is listed in the Key Resources Table.
- The glycopeptide microarray, fluorescence polarization data and trans-well migration data have been deposited in the general-purpose repository of Harvard Dataverse (DOI listed in the Key Resources Table)
- This paper does not report original code
- Any additional information required to reanalyze the data reported in this paper is available from the Lead Contact upon request.

EXPERIMENTAL MODEL AND SUBJECT DETAILS

Buffy coats were obtained from Rigshospitalet Copenhagen, as anonymous material, with written informed consent from the donors, and age and gender were not reported. The local ethics committee at Faculty of Health and Medical Sciences at the University of Copenhagen (Research Ethics Committee for Sund and Science, University of Copenhagen) found the project exempt from approval. The PBMCs used in the study were generated from pooled buffy coats.

METHOD DETAILS

A modified Glyco-SPOT synthesis method -—In order to produce a selection of glycosulfopeptides with defined acceptor sites and glycan structures, we modified the existing method of SPOT synthesis [50] and our recently published Glyco-SPOT method [36]. Main concerns were coupling efficiency of modified amino acids and the labile nature of tyrosine sulfates.

Safety Statement: The reagents used for the synthesis described herein are routinely used by most chemical laboratories and no unusually high safety hazards were encountered during these procedures. The following precautions were taken when handling the reagents used during the synthesis as most reagents used are rated to be flammable, toxic and/or corrosive. It is advisable to perform all steps in a certified chemical fume-hood, while wearing appropriate personal protective equipment. The use of flame and chemical resistant lab coats, along with chemical resistant disposable gloves with extended cuffs (such as

MICROFLEX® 93–260 from Ansell) and chemical safety goggles at all times is highly recommended. While pouring volatile solvents from large containers to smaller dispensing containers we used a chemical respirator.

Rationale for Sequences: The peptides synthesized were based on human and mouse PSGL-1, CCR7 and CCR10 sequences as controls.

Materials—Whatman® quantitative filter paper, hardened low-ash, Grade 50 (Cat #: WHA1450916), N-Methyl-2-Pyrrolidone (Biotech. grade, ≥99.7%) (Cat #: 494496–1L), 1-Hydroxybenzotriazole hydrate (HOBt) (wetted with not less than 14 wt. % water, 97%) (Cat #: 157260–100G), Bromophenol blue (Cat #: 114391–5G), were all purchased from Sigma-Aldrich (St. Louis, MO). Anhydrous amine-free N,N-Dimethylformamide (DMF) (Cat #: AA43465-K7) was purchased from VWR (Radnor, PA). N,N'-Diisopropylcarbodiimide (DIC) 99%, AcroSeal™, ACROS Organics™ (Cat #: AC446181000) was purchased from Fisher Scientific (Pittsburgh, PA). All regular Fmoc-protected amino acids were purchased from Novabiochem® a subsidiary of Millipore Sigma (Burlington, MA). FmocTyr(SO3nP)-OH (cat# 4082682) were purchased from Bachem. Fmoc-Thr(GalNAc(Ac)$_3$-α-D)-OH (Tn-Thr) (cat# GA131000), Fmoc-Thr(Galβ(1–3)GalNAc)-OH (Peracetate) (T-Thr) (cat# GA131010) and Fmoc-Thr(Galβ(1–3)(GlcNAcβ(1–6))GalNAc-OH (Peracetate) (core-2 Thr) (cat# GA131030) were purchased from Sussex Research (Ottawa, Ontario Canada). Recombinant GalNAc-T1 (cat # 7140-GT-020) was purchased from R&D Systems (Minneapolis, MN).

Box-shaped snap-lock type glass food container was purchased from the local retail store. Reusable biopsy punch (0.5mm tip) was purchased form World Precision Instruments (Sarasota, FL) (Cat #: 504639). Nexterion® Slide H 3D NHS (Schott) slides were purchased from Applied Microarrays (Tempe, AZ) (Cat #: 1070936). All other reagents and chemicals were purchased from either Sigma-Aldrich or Fisher Scientific and used without purification.

Preparation of the Membrane—The sheet of Whatman® quantitative filter paper was cut out as a rectangle and a grid was marked using a pencil such that each spot would lie within 1.6 cm × 1.6 cm square, and a 0.5 cm margin on all four sides of the sheet as empty space for fixing the sheet. The membrane was dried for ~60 minutes in a lyophilizer/vacuum desiccator at the end of the day prior to storage at −20°C and before each coupling step.

Testing NMP / DMF Solvent Quality before Synthesis—To achieve maximum efficiency for the reactions, the solvents must be free of any amines. Consequently, only amine-free and anhydrous grades of solvents should be used and aliquots of solvents taken during synthesis steps should be checked for amines using bromophenol blue test. For testing, 1 μL of 1% w/v bromophenol blue (in methanol) solution was added to 1 ml of solvent. If the color is green or blue, it indicates there is significant amines present and the solvent is discarded or used for final washes only. Yellow color test qualifies for coupling and blocking steps, where amine-free requirements are essential. To further ensure amine-free solvents, stock bottles and aliquot bottles should be flushed with anhydrous inert gas such as nitrogen or argon.

Coupling the first amino acid on to the paper—The filter paper was placed in the snap-lock container. 960 mg of Fmoc-Ala-OH was weighed and dissolved in 15 ml of NMP. Then 560 μL of DIC (N,N'-Diisopropylcarbodiimide) and 475 μL of 1-methylimidazole was added. The solution was poured into the glass container, closed and placed on a shaker overnight.

Amino acid solutions—For each cycle, 0.6 M HOBt dissolved in NMP and 1.8 M solution of DIC in NMP was prepared in bulk for each day. The final volume required to make a final concentration of 450 mM of amino acid solution was retrieved or calculated. The HOBt solution and DIC solution was added in a ratio of 3:1 HOBt solution : DIC solution to make the final volume. This gives a final concentration of 450 mM for the amino acids, HOBt and DIC. For FPGAs and sTyr which are more precious, the final concentrations used were 100 mM and appropriate calculations were done to have similar ratio of HOBt and DIC (100 mM each).

Spotting—For cycles in which only regular amino acids were used, the membrane was taped to a clear glass flat surface along the margins, and 1 μL of the amino acid mixture was deposited on the membrane. This was repeated for all the spots. The membrane was covered with a box-shaped glass food container placed upside down after a short flush with anhydrous inert gas nitrogen and allowed to incubate for 20 minutes.

Glyco-SulfoSpot Spotting—For spotting Glycoamino acids or tyrosine sulfates, the membrane was taped to the bottom of a sealable container. 1.5 μl of modified AA (FPGA or sTyr) was used for each spot, after all spots had been applied the container was filled with nitrogen gas and it was quickly sealed and incubated for 2 hr at room temperature. To increase coupling efficiency, a second coupling was performed by repeating the steps above and if required a third was also performed.

Blocking—The following capping solutions were prepared in sufficient volume so as to completely immerse the paper on which the synthesis is carried out.

Capping solution A: 1% acetic anhydride in amine-free DMF. Capping solution B: 1% acetic anhydride with 1% diisopropylethylamine (DIPEA) in amine-free DMF. Capping solution A was poured in glass snap-lock food container and the membrane was carefully placed upside down into the container using tweezers. The entire membrane must be submerged in the liquid, and the box handled with care to avoid any bubbles which could cause incomplete capping. The membrane was incubated for 2 minutes and solution A was then substituted for solution B. Carefully, with the use of tweezers, the membrane was lifted, turned face up and placed back into the container, while again avoiding air bubbles. The membrane was incubated for 5 minutes in solution B and then washed with 30 mL of amine-free DMF for 5 minutes while shaking (300 RPM, orbital shaker). After incubation, the solution was replaced with new DMF incubated for 60 seconds and repeated 2 additional times.

Fmoc deprotection—To de-protect the Fmoc groups, the membrane was incubated twice with 30 ml of 20% 4-methylpiperidine in DMF while shaking (300 RPM, orbital shaker) for 5 minutes. This was followed by 4 washes with methanol while shaking for 2 minutes each.

Quality check—To check the quality of individual synthesis step, a bromophenol blue stain was performed on the membrane after each coupling. 30 ml of 10 mg/L bromophenol blue in methanol was added to the membrane and shaken for approximately 30s (maximum 1 minute as permanent staining can occur which can be very troublesome to reverse and cause degradation). A blue color indicates that the free amine is present, and the coupling and Fmoc-deprotection steps were successful. To wash off the stain, methanol was added and the membrane shaken for 5 minutes. For several couplings, the stain would still be visible after this wash and 5 minutes with DMF and subsequent wash with methanol was required. The membrane was then dried in a vacuum desiccator and the next coupling was initiated or the membrane was frozen at −20°C for storage.

Biopsies—For a more detailed analysis of the synthesis, we removed a biopsy with a 0.5 mm diameter biopsy punch (World Precision Instruments Cat #504639) and analyzed with MALDI-TOF. For each analysis, we removed 2–3 biopsies from different spots on the membrane. Biopsies from each spot were pooled in individual Eppendorf tubes, de-protected (Global Side Chain Deprotection) and the peptides released as described below. After release, the solution was diluted in 1:10 in 50% ACN:Water with 0.1% TFA and directly spotted for MALDI analysis.

MALDI-TOF analysis of Peptides—We used MALDI-TOF in multiple steps to monitor the progress of synthesis, release, glycosylation reactions and to check the final purified peptides. Samples were diluted 1:50 in 50% acetonitrile and spotted on the MALDI plate and mixed 1:1 with DHB matrix (100 mg/mL in 50% acetonitrile). Spots were analyzed using linear negative mode, to monitor the tyrosine sulfate, approximately 1 – 2 sulfates were lost in the MALDI and therefore must be analyzed on HPLC in parallel to check for retention times (Table S2 and Figure S6). The MALDI is still useful to monitor relative changes in mass due to glycosylation and if sulfation is stable. We also observed a minor loss of sialic acid in the MALDI.

Peptide Side Chain Deprotection—To deprotect the side chain protecting groups of the amino acids without causing loss of sulfation we modified the methods previously used. The membrane was washed 4 times with 30 ml of dichloromethane (DCM) in the snap-lock glass food container before starting the deprotection. First, the membrane was treated with 50 ml of ice-cold solution A (TFA:TIPS:Water:Phenol:DCM :: 90:3:2:1:4) for 15 mins making sure there were no air bubbles and the membrane was completely covered with no shaking. In contrast to our previously published method [36] the incubation time for this step was shortened and carried out on ice to avoid hydrolysis of tyrosine sulfates. The membrane was then washed 3 times with 30 mL of DCM. In the second step, the membrane was treated with 50 ml of cleavage solution B (TFA:TIPS:Water:Phenol:DCM :: 50:3:2:1:44) for 2 hrs also on ice with no shaking. Lastly, the membrane was washed 4 times with 30 mL DCM followed by 4 times of Methanol wash, dried in a desiccator or lyophilizer for at least 5 hours to remove any residual trapped TFA and DCM.

Peptide Release—Peptides were released as previously described [36]: Briefly, a solution of 200 mM sodium bicarbonate was made in 1:2 methanol:water as the release solution.

Using sodium bicarbonate has the added advantage that it also removes the neopentyl protecting groups from the sulfotyrosines. The spots were cut out and placed in individual 2.0 ml microcentrifuge tubes. 1 ml of the release solution was added to the tubes, and mixed on a shaker for 5 minutes to neutralize any residual acids on the surface. This solution was discarded, and a fresh 1 ml of release solution was added to the tubes. The tubes were placed on an incubator shaker for 6–18 hrs at 30°C. We collected the solutions and stored them at −20°C or dried them immediately using a centrifugal evaporator.

Removal of additional acetyls—Following release, peptides were reconstituted in water and monitored by MALDI-TOF to ensure proper removal of side-chain protecting groups, neopentyls and acetyls. We observed that peptides containing Core-2 were resistant to removal of the acetyl protecting groups on the glycan, and still carried 2–3 acetyls, whereas acetyls on other FPGAs were removed during the release. To efficiently remove remaining acetyls for core-2 containing peptides, we incubated the peptides with 2.5% hydrazine for 2 hrs and reanalyzed with MALDI-TOF.

Enzymatic elongation—For generation of the different glycoforms we utilized a number of recombinant glycosyltransferases as depicted in Figure 1. Peptides were glycosylated in the following buffer: 50 mM Cacodylate, 10 mM $MnCl_2$, 1 mM $CaCl_2$, and pH: 7.2. We resuspended peptides in reaction buffer to a final concentration of 5 mg/mL or less with sugar nucleotides (UDP-GalNAc, UDP-Galactose, CMP-Sialic acid, GDP-Fucose) at a final concentration of 10mM. We then added recombinant glycosyl-transferases (Cosmc, T-Synthase, ST6GalNAc1, GCNT1, FUT6, β1,4GalT, ST3Gal4, ST3Gal1) in a ratio of 1:50 relative to peptide amount. Reactions were incubated at 37°C for 2 hrs and monitored by MALDI TOF and HPLC (see Figure S6). If reactions were not complete, they were spiked with additional enzyme and sugar donor. All reactions with ST3Gal4 were spiked and incubated overnight at 37°C. When the MALDI analysis showed completion of the enzymatic reactions, solutions were de-salted using C18 Sep-Pak. The columns were first washed with 1 column volume (CV) Buffer A (20 mM ammonium acetate pH 6.5), activated with 1 CV Buffer B (20 mM ammonium acetate with 70% acetonitrile pH 6.5) and washed with 3 CV of Buffer A. Sample (enzyme reaction) was diluted 1:10 in Buffer A and loaded onto the column, flow through was loaded one time. The column was then washed with 1 CV of water and eluted in 50% acetonitrile. Finally, the eluates were dried on a centrifugal evaporator (SpeedVac™).

HPLC analysis and purification—For analysis or purification, we performed HPLC experiments on a Shimadzu HPLC equipped with a fluorescence detector, using a Phenomenex Kinetex C18 column. The buffer system consisted of: Buffer A (20 mM Ammonium acetate pH 6.5) and Buffer B (20 mM ammonium acetate with 70% Acetonitrile pH 6.5). Signals were detected based on fluorescence from the *N*-terminal fluorescein and fractions collected accordingly (Figure S6).

Quantification of Peptides—The peptides were quantified by measuring the absorbance at 453 nm for the fluorescein. Previously, it has been shown that the absorption maximum for fluorescein at pH 6.5 is at 453 nm with a molar absorptivity of 29,000 $M^{-1}cm^{-1}$ [51]. As

a result, we dissolved the compounds in pH 6.5 buffer and quantified using a Nanodrop, adding 2 μL of sample as instructed in the user manual.

Microarray Printing—Arrays were printed using sciFLEXARRAYER S11 microarray printer (Scienion) onto Nexterion® Slide H 3D NHS (Schott) slides. Briefly, the peptides were diluted into PBS (phosphate buffered saline) buffer pH 7.4 at 100 μM concentrations for printing. Following this, the peptides were transferred into a 384-well polypropylene microplate which can be interfaced with the instrument. The printer was used with the PDC 70 Type 3 nozzles (70 μm inner diameter) and the voltage and pulse parameters were adjusted to dispense 330 pl per spot. All samples were printed as 4 spots on individual arrays in 8-subarray per slide format (dimensions based on Grace Biolabs ProPlate® Multi-Well Chambers). Following the printing, the slides were incubated overnight at room temperature at 70% humidity and then blocked with 50 mM ethanolamine in 100 mM borate buffer for 1 hr (pH 8.0), dip washed 10 times in PBS and then 10 times in water. The slides were then centrifuged to dry in a slide centrifuge, prior to storage at −20°C.

Microarray Assays—To perform microarray assays, the slides were removed from the freezer and stored in a desiccator to bring to room temperature for the assay. The following buffers were prepared: TSM buffer (20 mM Tris-HCl, pH 7.4, 150 mM NaCl, 2 mM CaCl2, 2 mM MgCl2), TSM Wash Buffer (TSMW) (TSM Buffer + 0.05% Tween-20), TSM Binding Buffer (TSMBB) (TSM buffer + 0.05% Tween 20 + 1% BSA-protease free), TSM Binding Buffer with extra calcium (TSM buffer with 10 mM CaCl2 + 0.05% Tween 20 + 1% BSA-protease free), TSM Binding Buffer with no calcium (TSM buffer plus EDTA + 0.05% Tween 20 + 1% BSA-protease free). The 16-well ProPlate® Multi-Well Chambers (Grace Biolabs) were fitted as per manufacturer's instructions. Following this the wells in which the assay was to be performed were rehydrated using TSM Wash (TSMW) buffer for 5 minutes. The following samples were incubated on the array: human P-selectin (R&D Systems) (5 μg/mL in TSMBB with 10 mM calcium chloride buffer pH 8.0, and also tested in TSMBB no calcium plus EDTA buffer), mouse P-selectin (R&D Systems) (5 μg/ml) human E-selectin (R&D Systems) (5 μg/mL). Selectins were produced as human Fc-chimeras. Detection of selectins was accomplished by incubating with Alexa Fluor-647-labeled anti-human IgG (5 μg/mL in TSMBB). CCL5, CCL19 and CCL21 were from R&D systems and was used at in TSMBB. Binding of chemokines was performed using either 1 μg/mL of recombinant CCL5 (R&D systems), recombinant CCL19 (R&D systems) and CCL21 (R&D systems). Detection was performed with 1 μg/mL of mouse anti-human CCL5/RANTES antibody, human CCL19/MIP-3 beta antibody (cat# AF361), human CCL21/6Ckine antibody (cat# AF366) and Alexa Fluor-647-labeled secondary anti-goat in TSMBB. Biotinylated lectins *Vicia villosa* agglutinin (VVA) and *Aleuria aurantia* lectin (AAL) from Vector labs were used at 20 μg/mL and detected with 1 μg/mL streptavidin-Cy5 in TSMBB. KPL1 antibody (Santa Cruz # sc-13535) to PSGL-1 peptide was used at 5 μg/mL in TSMBB. The slide was subsequently washed in TSMW buffer 5 times, followed by water 5 times, and centrifuged to dry.

The slides were scanned using a GenePix 4300A or 4400A microarray scanner (Molecular Devices). The scan settings used in the scanner were: resolution 10 μm/pixel, PMT gain 500,

scan power 90, wavelength 488 with standard blue filter or 635 with Cy5 filter. The scan settings were kept identical for all samples so as to make the data more comparable. The spots were aligned, and relative fluorescent intensities (RFU) quantified using the GenePix Pro software and data was processed using Microsoft Excel to average the intensities for all spots of a specific probe to obtain the mean RFU values which are plotted in the figures shown, along with the standard deviation of the 4 spots.

Fluorescence Polarization Assay—Assays were done in black low volume 384 well plates from Greiner. Recombinant chemokines were purchased from Chemotactics Inc. (Carlsbad, CA) and resuspended in FP buffer (1:3 PBS and MilliQ water). PSGL-1 peptides were diluted in FP buffer to a final concentration of 100nM. Chemokines were added to a 384-well plate and diluted 2-fold dilutions series from 1μM to 0.12nM and the plates were sealed to prevent evaporation. Plates were incubated for 20 minutes at room temperature, centrifuged and mFP were measured using a Flexstation 3 (Molecular devices). Experiments were performed in triplicates. Data was analyzed and plotted with Excel and GraphPad Prism using a nonlinear fit to obtain kd values.

Preparation of Human Dendritic Cells—We obtained buffy coats from healthy donors (Rigshospitalet, Copenhagen, Denmark) designated as anonymous material and approved by the local ethics committee. We isolated human peripheral blood mononuclear cells (PBMC) from buffy coats by density gradient centrifugation using Lymphoprep™ (Stemcell Technologies). From this subpopulation we isolated monocytes by plastic adherence. We then cultured the adhered monocytes and differentiated them into immature dendritic cells (DCs) by incubation with IL-4 (250U/ml) and GM-CSF (1000U/ml) for 6 days. The immature human DCs were then cultured in X-VIVO™ 15 medium (Lonza) with 2% human AB serum and glutamine.

Trans-Well Migration Assay—200,000 immature dendritic cells were seeded in the upper chamber of a 6.5 mm Transwell with 5.0 μm pore polycarbonate membrane insert (Corning cat#CLS3421). In the lower chamber serum free media with 3 nM CCL19, 5 nM CCL21 or media only were added with sulfopeptide unmodified peptide or no peptide. Cells were incubated for 2 hrs, and the lower chamber was collected and migration was assayed by adding CellTiter-Glo® (Promega), reading luminescence on Flexstation 3 (Molecular Devices) and calculating migrated cells in Microsoft Excel.

MS/MS analysis—Two μg recombinant PSGL-1 (R&D Systems) were treated with 2 μL neuraminidase (Roche, #10269611001), 2 μL β1–3 galactosidase (NEB, #P0726S) and 2 μL β1–4 galactosidase (NEB, #P0745L) in 50mM sodium acetate, 5mM CaCl2, pH5.5 and incubated at 37°C overnight according to the manufacturers instruction (NEB). The samples subjected to in-gel PNGase F and subsequent trypsin or AspN treatment as described elsewhere [52]. Two μL of each sample were used for C18-reversed phase-liquid chromatography-mass spectrometry analysis (C18-RP-LC-MS/MS) using an Ultimate 3000 nano LC coupled to an Orbitrap Fusion Lumos mass spectrometer (both Thermo Fisher) as described elsewhere [27].

Glycopeptide identification was performed using Byonic version 3.5 (Protein Metrics Inc.). Trypsin or AspN were set a protease with a maximum of two missed cleavage sites, the precursor and fragment mass tolerance was 10 ppm. The glycan database contained core 1 and core 2 O-glycans. The following modifications were allowed: carbamidomethyl (Cys; fixed), oxidation (Met; variable common 1), pyroglutamine on N-term (Gln, variable, rare 1), deamidation (Asn, variable common 1), formylation N-term (variable rare 1), ammonia-loss N-term (Cys, variable rare1), sulfation (Tyr, fixed). Glycopeptides with a score above 250 were selected and further manually inspected.

QUANTIFICATION AND STATISTICAL ANALYSIS

For the microarrays, the peptides were printed as 4 spots/array and the average of the mean RFU – background was taken (n=4). The error bars represent standard deviations. The data was analyzed using Excel.

For the trans-well migration assays, the average of 4 points was taken (n=4) and the standard deviation calculated. The significance was calculated based on t-test.

For the fluorescence polarization assay the experiments were done in triplicates and the average was taken (n=3). The data was analyzed and plotted with Excel and GraphPad Prism using a nonlinear fit to obtain kd values.

Supplementary Material

Refer to Web version on PubMed Central for supplementary material.

Acknowledgements

This work was support by the independent research fund Denmark (7025–00083B) to C.K.G and the Lundbeck Foundation (R322–2019-2171) to C.K.G., and by NIH grants P41GM103694 and R24GM137763 to R.D.C.

References

1. Mehta P, Cummings RD, and McEver RP (1998). Affinity and kinetic analysis of P-selectin binding to P-selectin glycoprotein ligand-1. J. Biol. Chem. 273, 32506–32513. 10.1074/jbc.273.49.32506. [PubMed: 9829984]
2. Moore KL, Patel KD, Bruehl RE, Li F, Johnson DA, Lichenstein HS, Cummings RD, Bainton DF, and McEver RP (1995). P-selectin glycoprotein ligand-1 mediates rolling of human neutrophils on P-selectin. J. Cell Biol. 128, 661–671. 10.1083/jcb.128.4.661. [PubMed: 7532174]
3. Vachino G, Chang XJ, Veldman GM, Kumar R, Sako D, Fouser LA, Berndt MC, and Cumming DA (1995). P-selectin glycoprotein ligand-1 is the major counter-receptor for P-selectin on stimulated T cells and is widely distributed in non-functional form on many lymphocytic cells. J. Biol. Chem. 270, 21966–21974. 10.1074/jbc.270.37.21966. [PubMed: 7545173]
4. Xia L, Sperandio M, Yago T, McDaniel JM, Cummings RD, Pearson-White S, Ley K, and McEver RP (2002). P-selectin glycoprotein ligand-1-deficient mice have impaired leukocyte tethering to E-selectin under flow. J. Clin. Invest. 109, 939–950. 10.1172/JCI14151. [PubMed: 11927621]
5. Tinoco R, and Bradley LM (2017). Targeting the PSGL-1 pathway for immune modulation. Immunotherapy 9, 785–788. 10.2217/imt-2017-0078. [PubMed: 28877633]
6. Krishnamurthy VR, Sardar MY, Ying Y, Song X, Haller C, Dai E, Wang X, Hanjaya-Putra D, Sun L, Morikis V, et al. (2015). Glycopeptide analogues of PSGL-1 inhibit P-selectin in vitro and in vivo. Nat Commun 6, 6387. 10.1038/ncomms7387. [PubMed: 25824568]

7. Chaikof EL, Wong DJ, Park DD, Park SS, Haller C, Chen J, Dai E, Liu L, Mandhapati AR, Eradi P, et al. (2021). A PSGL-1 Glycomimetic Reduces Thrombus Burden Without Affecting Hemostasis. Blood. 10.1182/blood.2020009428.
8. Tauxe C, Xie X, Joffraud M, Martinez M, Schapira M, and Spertini O (2008). P-selectin glycoprotein ligand-1 decameric repeats regulate selectin-dependent rolling under flow conditions. J. Biol. Chem. 283, 28536–28545. 10.1074/jbc.M802865200. [PubMed: 18713749]
9. Wilkins PP, McEver RP, and Cummings RD (1996). Structures of the O-glycans on P-selectin glycoprotein ligand-1 from HL-60 cells. J. Biol. Chem. 271, 18732–18742. 10.1074/jbc.271.31.18732. [PubMed: 8702529]
10. Li F, Wilkins PP, Crawley S, Weinstein J, Cummings RD, and McEver RP (1996). Post-translational modifications of recombinant P-selectin glycoprotein ligand-1 required for binding to P- and E-selectin. J. Biol. Chem. 271, 3255–3264. [PubMed: 8621728]
11. Wilkins PP, Moore KL, McEver RP, and Cummings RD (1995). Tyrosine sulfation of P-selectin glycoprotein ligand-1 is required for high affinity binding to P-selectin. J. Biol. Chem. 270, 22677–22680. 10.1074/jbc.270.39.22677. [PubMed: 7559387]
12. Leppanen A, Mehta P, Ouyang YB, Ju T, Helin J, Moore KL, van Die I, Canfield WM, McEver RP, and Cummings RD (1999). A novel glycosulfopeptide binds to P-selectin and inhibits leukocyte adhesion to P-selectin. J. Biol. Chem. 274, 24838–24848. 10.1074/jbc.274.35.24838. [PubMed: 10455156]
13. Leppanen A, White SP, Helin J, McEver RP, and Cummings RD (2000). Binding of glycosulfopeptides to P-selectin requires stereospecific contributions of individual tyrosine sulfate and sugar residues. J. Biol. Chem. 275, 39569–39578. 10.1074/jbc.M005005200. [PubMed: 10978329]
14. Tinoco R, Carrette F, Barraza ML, Otero DC, Magana J, Bosenberg MW, Swain SL, and Bradley LM (2016). PSGL-1 Is an Immune Checkpoint Regulator that Promotes T Cell Exhaustion. Immunity 44, 1470. 10.1016/j.immuni.2016.05.011. [PubMed: 27332735]
15. Xu T, Zhang L, Geng ZH, Wang HB, Wang JT, Chen M, and Geng JG (2007). P-selectin cross-links PSGL-1 and enhances neutrophil adhesion to fibrinogen and ICAM-1 in a Src kinase-dependent, but GPCR-independent mechanism. Cell Adh Migr 1, 115–123. 10.4161/cam.1.3.4984. [PubMed: 19262138]
16. Urzainqui A, Martinez del Hoyo G, Lamana A, de la Fuente H, Barreiro O, Olazabal IM, Martin P, Wild MK, Vestweber D, Gonzalez-Amaro R, and Sanchez-Madrid F (2007). Functional role of P-selectin glycoprotein ligand 1/P-selectin interaction in the generation of tolerogenic dendritic cells. J. Immunol. 179, 7457–7465. 10.4049/jimmunol.179.11.7457. [PubMed: 18025190]
17. Hirata T, Furukawa Y, Yang BG, Hieshima K, Fukuda M, Kannagi R, Yoshie O, and Miyasaka M (2004). Human P-selectin glycoprotein ligand-1 (PSGL-1) interacts with the skin-associated chemokine CCL27 via sulfated tyrosines at the PSGL-1 amino terminus. J. Biol. Chem. 279, 51775–51782. 10.1074/jbc.M409868200. [PubMed: 15466853]
18. Veerman KM, Williams MJ, Uchimura K, Singer MS, Merzaban JS, Naus S, Carlow DA, Owen P, Rivera-Nieves J, Rosen SD, and Ziltener HJ (2007). Interaction of the selectin ligand PSGL-1 with chemokines CCL21 and CCL19 facilitates efficient homing of T cells to secondary lymphoid organs. Nat. Immunol. 8, 532–539. 10.1038/ni1456. [PubMed: 17401367]
19. Veldkamp CT, Kiermaier E, Gabel-Eissens SJ, Gillitzer ML, Lippner DR, DiSilvio FA, Mueller CJ, Wantuch PL, Chaffee GR, Famiglietti MW, et al. (2015). Solution Structure of CCL19 and Identification of Overlapping CCR7 and PSGL-1 Binding Sites. Biochemistry 54, 4163–4166. 10.1021/acs.biochem.5b00560. [PubMed: 26115234]
20. Steen A, Larsen O, Thiele S, and Rosenkilde MM (2014). Biased and g protein-independent signaling of chemokine receptors. Front. Immunol. 5, 277. 10.3389/fimmu.2014.00277. [PubMed: 25002861]
21. Solari R, Pease JE, and Begg M (2015). “Chemokine receptors as therapeutic targets: Why aren’t there more drugs?”. Eur. J. Pharmacol. 746, 363–367. 10.1016/j.ejphar.2014.06.060. [PubMed: 25016087]
22. Ludeman JP, and Stone MJ (2014). The structural role of receptor tyrosine sulfation in chemokine recognition. Br. J. Pharmacol. 171, 1167–1179. 10.1111/bph.12455. [PubMed: 24116930]

23. Stone MJ, and Payne RJ (2015). Homogeneous sulfopeptides and sulfoproteins: synthetic approaches and applications to characterize the effects of tyrosine sulfation on biochemical function. Acc. Chem. Res. 48, 2251–2261. 10.1021/acs.accounts.5b00255. [PubMed: 26196117]

24. Jung SA, Jin S, Chae JB, Jo G, Chung H, Lyu J, and Lee JH (2021). Recombinant sulfated CCR2 peptide trap reduces retinal degeneration in mice. Biochem. Biophys. Res. Commun. 572, 171–177. 10.1016/j.bbrc.2021.08.002. [PubMed: 34371259]

25. Bannert N, Craig S, Farzan M, Sogah D, Santo NV, Choe H, and Sodroski J (2001). Sialylated O-glycans and sulfated tyrosines in the NH2-terminal domain of CC chemokine receptor 5 contribute to high affinity binding of chemokines. J. Exp. Med. 194, 1661–1673. [PubMed: 11733580]

26. Kiermaier E, Moussion C, Veldkamp CT, Gerardy-Schahn R, de Vries I, Williams LG, Chaffee GR, Phillips AJ, Freiberger F, Imre R, et al. (2016). Polysialylation controls dendritic cell trafficking by regulating chemokine recognition. Science 351, 186–190. 10.1126/science.aad0512. [PubMed: 26657283]

27. Zeng J, Eljalby M, Aryal RP, Lehoux S, Stavenhagen K, Kudelka MR, Wang Y, Wang J, Ju T, von Andrian UH, and Cummings RD (2020). Cosmc controls B cell homing. Nat Commun 11, 3990. 10.1038/s41467-020-17765-6. [PubMed: 32778659]

28. Hauser MA, Kindinger I, Laufer JM, Spate AK, Bucher D, Vanes SL, Krueger WA, Wittmann V, and Legler DF (2016). Distinct CCR7 glycosylation pattern shapes receptor signaling and endocytosis to modulate chemotactic responses. J. Leukoc. Biol. 99, 993–1007. 10.1189/jlb.2VMA0915-432RR. [PubMed: 26819318]

29. Mehta AY, Heimburg-Molinaro J, Cummings RD, and Goth CK (2020). Emerging patterns of tyrosine sulfation and O-glycosylation cross-talk and co-localization. Curr. Opin. Struct. Biol. 62, 102–111. 10.1016/j.sbi.2019.12.002. [PubMed: 31927217]

30. Okamoto Y, and Shikano S (2021). Tyrosine sulfation and O-glycosylation of chemoattractant receptor GPR15 differentially regulate interaction with GPR15L. J. Cell Sci. 134. 10.1242/jcs.247833.

31. Cummings RD (2019). “Stuck on sugars - how carbohydrates regulate cell adhesion, recognition, and signaling”. Glycoconj. J. 36, 241–257. 10.1007/s10719-019-09876-0. [PubMed: 31267247]

32. Lee-Sundlov MM, Ashline DJ, Hanneman AJ, Grozovsky R, Reinhold VN, Hoffmeister KM, and Lau JT (2017). Circulating blood and platelets supply glycosyltransferases that enable extrinsic extracellular glycosylation. Glycobiology 27, 188–198. 10.1093/glycob/cww108. [PubMed: 27798070]

33. Rodriguez-Walker M, Vilcaes AA, Garbarino-Pico E, and Daniotti JL (2015). Role of plasma-membrane-bound sialidase NEU3 in clathrin-mediated endocytosis. Biochem. J. 470, 131–144. 10.1042/BJ20141550. [PubMed: 26251452]

34. Mishiro E, Sakakibara Y, Liu MC, and Suiko M (2006). Differential enzymatic characteristics and tissue-specific expression of human TPST-1 and TPST-2. J. Biochem. 140, 731–737. 10.1093/jb/mvj206. [PubMed: 17028309]

35. Lee RW, and Huttner WB (1983). Tyrosine-O-sulfated proteins of PC12 pheochromocytoma cells and their sulfation by a tyrosylprotein sulfotransferase. J. Biol. Chem. 258, 11326–11334. [PubMed: 6577005]

36. Mehta AY, Veeraiah RKH, Dutta S, Goth CK, Hanes MS, Gao C, Stavenhagen K, Kardish R, Matsumoto Y, Heimburg-Molinaro J, et al. (2020). Parallel Glyco-SPOT Synthesis of Glycopeptide Libraries. Cell Chem Biol. 10.1016/j.chembiol.2020.06.007.

37. Jorgensen AS, Brandum EP, Mikkelsen JM, Orfin KA, Boilesen DR, Egerod KL, Moussouras NA, Vilhardt F, Kalinski P, Basse P, et al. (2021). The C-terminal peptide of CCL21 drastically augments CCL21 activity through the dendritic cell lymph node homing receptor CCR7 by interaction with the receptor N-terminus. Cell. Mol. Life Sci. 78, 6963–6978. 10.1007/s00018-021-03930-7. [PubMed: 34586443]

38. Seibert C, Sanfiz A, Sakmar TP, and Veldkamp CT (2016). Preparation and Analysis of N-Terminal Chemokine Receptor Sulfopeptides Using Tyrosylprotein Sulfotransferase Enzymes. Methods Enzymol. 570, 357–388. 10.1016/bs.mie.2015.09.004. [PubMed: 26921955]

39. Steentoft C, Vakhrushev SY, Joshi HJ, Kong Y, Vester-Christensen MB, Schjoldager KT, Lavrsen K, Dabelsteen S, Pedersen NB, Marcos-Silva L, et al. (2013). Precision mapping of the human

O-GalNAc glycoproteome through SimpleCell technology. EMBO J. 32, 1478–1488. 10.1038/emboj.2013.79. [PubMed: 23584533]

40. Wong DJ, Park DD, Park SS, Haller CA, Chen J, Dai E, Liu L, Mandhapati AR, Eradi P, Dhakal B, et al. (2021). A PSGL-1 glycomimetic reduces thrombus burden without affecting hemostasis. Blood 138, 1182–1193. 10.1182/blood.2020009428. [PubMed: 33945603]
41. Dyer DP, Salanga CL, Volkman BF, Kawamura T, and Handel TM (2016). The dependence of chemokine-glycosaminoglycan interactions on chemokine oligomerization. Glycobiology 26, 312–326. 10.1093/glycob/cwv100. [PubMed: 26582609]
42. Zhu JZ, Millard CJ, Ludeman JP, Simpson LS, Clayton DJ, Payne RJ, Widlanski TS, and Stone MJ (2011). Tyrosine sulfation influences the chemokine binding selectivity of peptides derived from chemokine receptor CCR3. Biochemistry 50, 1524–1534. 10.1021/bi101240v. [PubMed: 21235238]
43. Johnston RJ, Su LJ, Pinckney J, Critton D, Boyer E, Krishnakumar A, Corbett M, Rankin AL, Dibella R, Campbell L, et al. (2019). VISTA is an acidic pH-selective ligand for PSGL-1. Nature 574, 565–570. 10.1038/s41586-019-1674-5. [PubMed: 31645726]
44. Bundgaard JR, Vuust J, and Rehfeld JF (1995). Tyrosine O-sulfation promotes proteolytic processing of progastrin. EMBO J. 14, 3073–3079. [PubMed: 7621822]
45. Farzan M, Mirzabekov T, Kolchinsky P, Wyatt R, Cayabyab M, Gerard NP, Gerard C, Sodroski J, and Choe H (1999). Tyrosine sulfation of the amino terminus of CCR5 facilitates HIV-1 entry. Cell 96, 667–676. [PubMed: 10089882]
46. Hintze J, Ye Z, Narimatsu Y, Madsen TD, Joshi HJ, Goth CK, Linstedt A, Bachert C, Mandel U, Bennett EP, et al. (2018). Probing the contribution of individual polypeptide GalNAc-transferase isoforms to the O-glycoproteome by inducible expression in isogenic cell lines. J. Biol. Chem. 293, 19064–19077. 10.1074/jbc.RA118.004516. [PubMed: 30327431]
47. Narimatsu Y, Joshi HJ, Nason R, Van Coillie J, Karlsson R, Sun L, Ye Z, Chen YH, Schjoldager KT, Steentoft C, et al. (2019). An Atlas of Human Glycosylation Pathways Enables Display of the Human Glycome by Gene Engineered Cells. Mol. Cell 75, 394–407 e395. 10.1016/j.molcel.2019.05.017. [PubMed: 31227230]
48. Bull C, Nason R, Sun L, Van Coillie J, Madriz Sorensen D, Moons SJ, Yang Z, Arbitman S, Fernandes SM, Furukawa S, et al. (2021). Probing the binding specificities of human Siglecs by cell-based glycan arrays. Proc. Natl. Acad. Sci. U. S. A. 118. 10.1073/pnas.2026102118.
49. Italia JS, Peeler JC, Hillenbrand CM, Latour C, Weerapana E, and Chatterjee A (2020). Genetically encoded protein sulfation in mammalian cells. Nat. Chem. Biol. 16, 379–382. 10.1038/s41589-020-0493-1. [PubMed: 32198493]
50. Hilpert K, Winkler DF, and Hancock RE (2007). Peptide arrays on cellulose support: SPOT synthesis, a time and cost efficient method for synthesis of large numbers of peptides in a parallel and addressable fashion. Nat. Protoc. 2, 1333–1349. 10.1038/nprot.2007.160. [PubMed: 17545971]
51. Sjöback R, Nygren J, and Kubista M (1995). Absorption and fluorescence properties of fluorescein. Spectrochimica Acta Part A: Molecular and Biomolecular Spectroscopy 51, L7–L21.
52. Stavenhagen K, Plomp R, and Wuhrer M (2015). Site-Specific Protein N- and O-Glycosylation Analysis by a C18-Porous Graphitized Carbon-Liquid Chromatography-Electrospray Ionization Mass Spectrometry Approach Using Pronase Treated Glycopeptides. Anal. Chem. 87, 11691–11699. 10.1021/acs.analchem.5b02366. [PubMed: 26536155]
53. Aryal RP, Ju T, and Cummings RD (2010). The endoplasmic reticulum chaperone Cosmc directly promotes *in vitro* folding of T-synthase. J. Biol. Chem. 285, 2456–2462. 10.1074/jbc.M109.065169. [PubMed: 19923218]
54. Hanes MS, Moremen KW, and Cummings RD (2017). Biochemical characterization of functional domains of the chaperone Cosmc. PLoS One 12, e0180242. 10.1371/journal.pone.0180242. [PubMed: 28665962]
55. Moremen KW, Ramiah A, Stuart M, Steel J, Meng L, Forouhar F, Moniz HA, Gahlay G, Gao Z, Chapla D, et al. (2018). Expression system for structural and functional studies of human glycosylation enzymes. Nat. Chem. Biol. 14, 156–162. 10.1038/nchembio.2539. [PubMed: 29251719]

Significance

Our study provides novel insight into the regulation of CCL19 and CCL21 binding by PSGL-1 demonstrating that O-glycan branching and sialylation status negatively affects the binding. We also expand the possible chemokine ligands for PSGL-1 and propose that Thr44 is potentially O-glycosylated and is involved in chemokine regulation. We have developed a new method and have produced a systematic and comprehensive library of novel PSGL-1 glycosulfopeptides and corresponding microarray. The method for synthesis can be easily implemented in laboratories without expensive instrumentation and can be scaled to microgram (nmol) scale. The strategy can be readily applied to other proteins of interest and represent a significant advancement for the dissection of the emerging patterns of co-localization of O-glycosylation and tyrosine sulfation.

Highlights

- >50 PSGL-1 N-terminus glycosulfopeptides were chemoenzymatically synthesized
- Identified role of post-translational modifications on PSGL-1 chemokine interaction
- Tyrosine sulfation of glycosulfopeptides positively affects CCL19 and CCL21 binding
- O-glycan branching and sialylation of glycosulfopeptides reduces chemokine binding

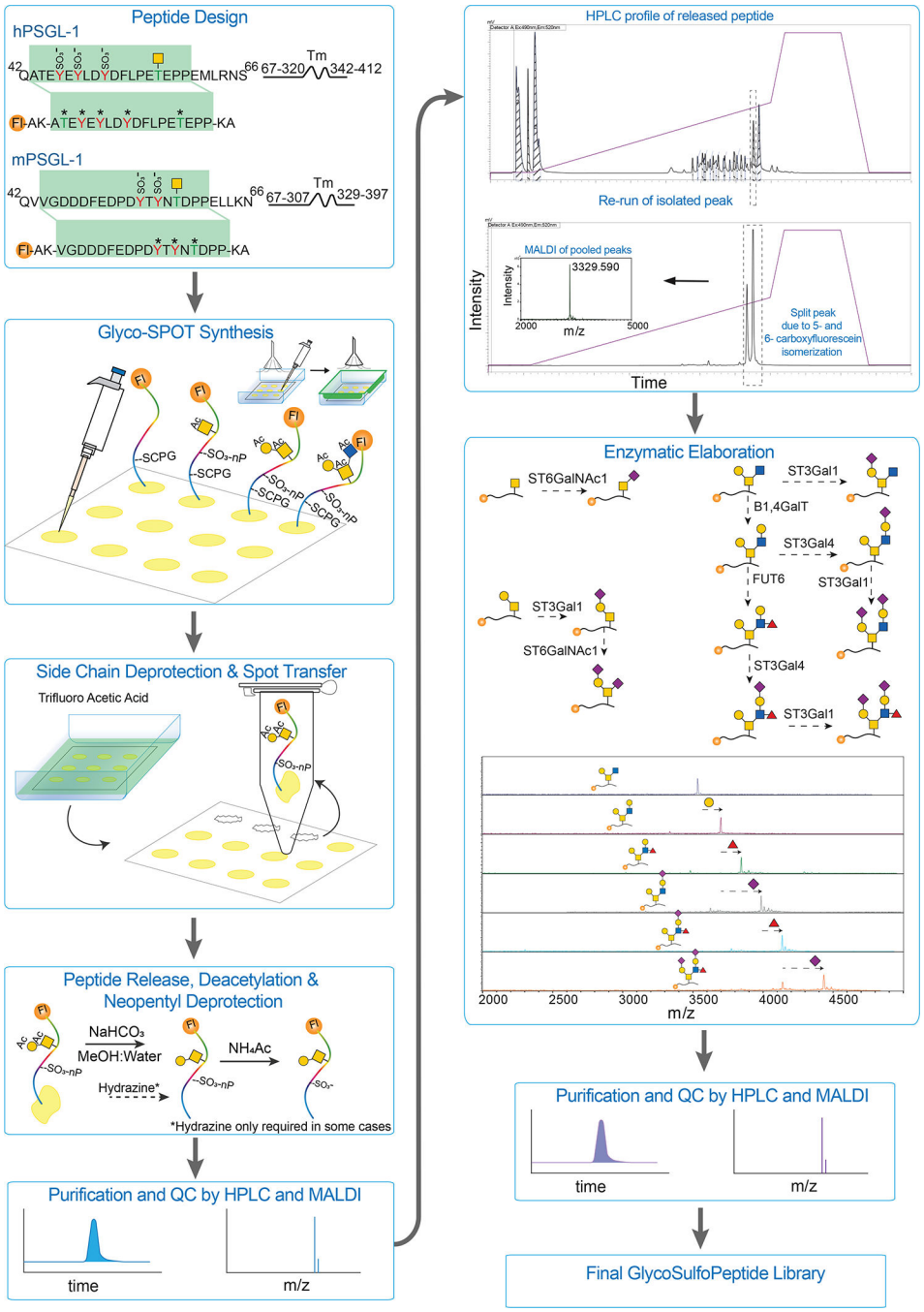

Figure 1. Schematic overview of modified Glyco-SPOT synthesis

Peptide design based on the PSGL-1 sequence of human (hPSGL-1) and murine (mPSGL-1), with C-terminal and N-terminal lysines appended for bidirectional printing of peptides, and designed with N-terminal fluorescein 5(6)-FAM for downstream applications. Peptides synthesized on cellulose paper using regular Fmoc protected amino acids, Fmoc-Tyr(SO_3nP) or Fmoc-threonine with peracetylated GalNAc, core 1 or core 2. After complete synthesis, side chains were deprotected, peptide spots were cut out and peptides released by incubating with sodium bicarbonate in MeOH, which removed the neopentyls from sulfated

tyrosines. Peptides were purified by HPLC and characterized on MALDI. O-glycans were elongated with a set of recombinant glycosyltransferases followed by MALDI and purified and analyzed again, to generate the final collection of structures.

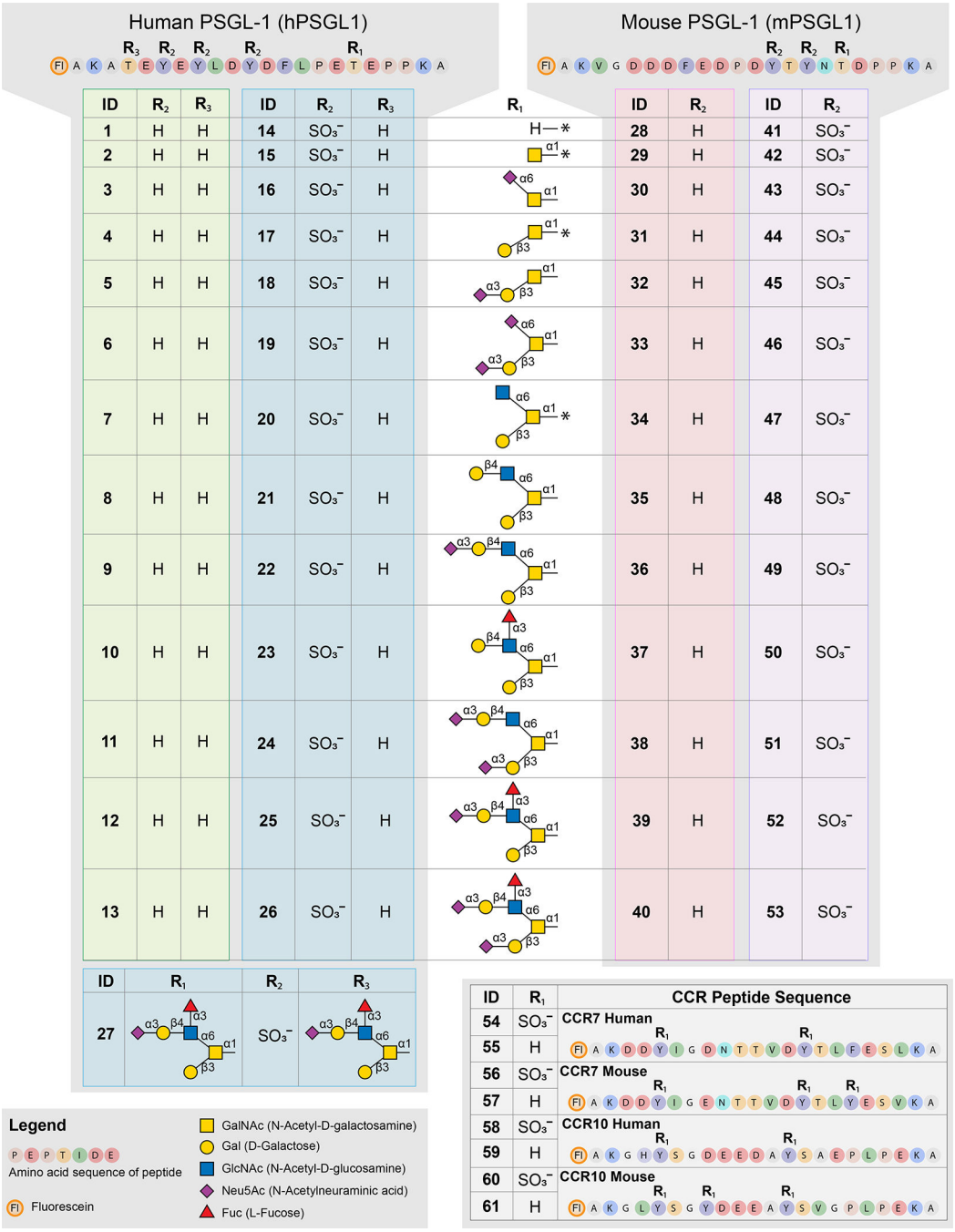

Figure 2. Overview of peptides and modifications

All synthesized peptides in the glycosulfopeptide library were assigned an ID number from 1 to 61, starting with the human PSGL-1 sequences (1–27), the murine PSGL-1 sequences (28–53) and finally the CCR7 and CCR10 peptides (54–61). Peptides were synthesized with and without glycosylation on R1 (corresponding to threonine 57 in full length human PSGL-1 and threonine 58 in murine PSGL-1). Glycans were extended to the different structures depicted in the middle panel. PSGL-1 peptides either carried no sulfation (1–13 shown in green, 28–40 shown in red) or were sulfated on all tyrosines on R2 (14–27 in blue,

41–53 shown in purple). One human PSGL-1 peptide carrying two SLe^x structures (also denoted 2 X SLe^x) and three tyrosine sulfates (27 shown in lower left) was also generated. All CCR peptides were synthesized without glycosylation and with or without sulfation on all tyrosines designated R1 (shown in lower right). A complete list is shown in Table S1.

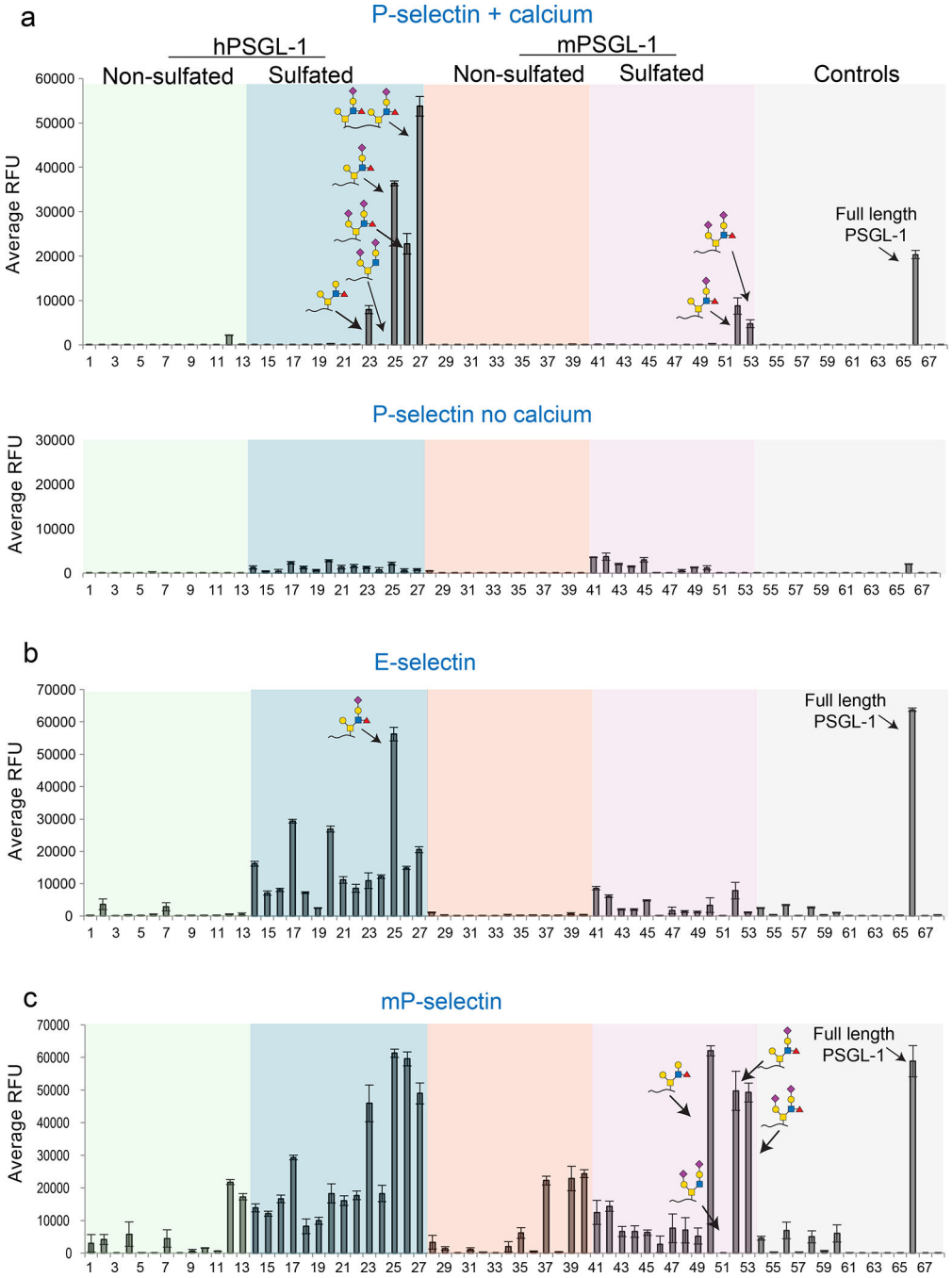

Figure 3. P-selectin binding to the glycosulfopeptide PSGL-1 microarray

a) Glycosulfopeptide PSGL-1 microarray probed with human P-selectin-Fc chimera (hP-selectin) (5 μg/mL) with (top) and without (bottom) calcium in the binding buffer. In the presence of calcium, hP-selectin exhibits binding to sulfated human and mouse PSGL-1 peptides carrying SLe^x (25), di-sialyl-Le^x (26), and human 2 X SLe^x (27) peptide as well as the recombinant full length PSGL-1 protein (66). b) Human E-selectin (5 μg/mL) showed broader specificity binding to most human sulfated peptides, with SLe^x peptide (25) exhibiting highest binding. c) Like hP-selectin, mP-selectin (5 μg/mL) exhibited cross-

species binding to sulfated PSGL-1 peptides. y-axis = relative fluorescent units (RFU), error bars = +/− 1 standard deviation. Color coding in graphs matches with Figure 2.

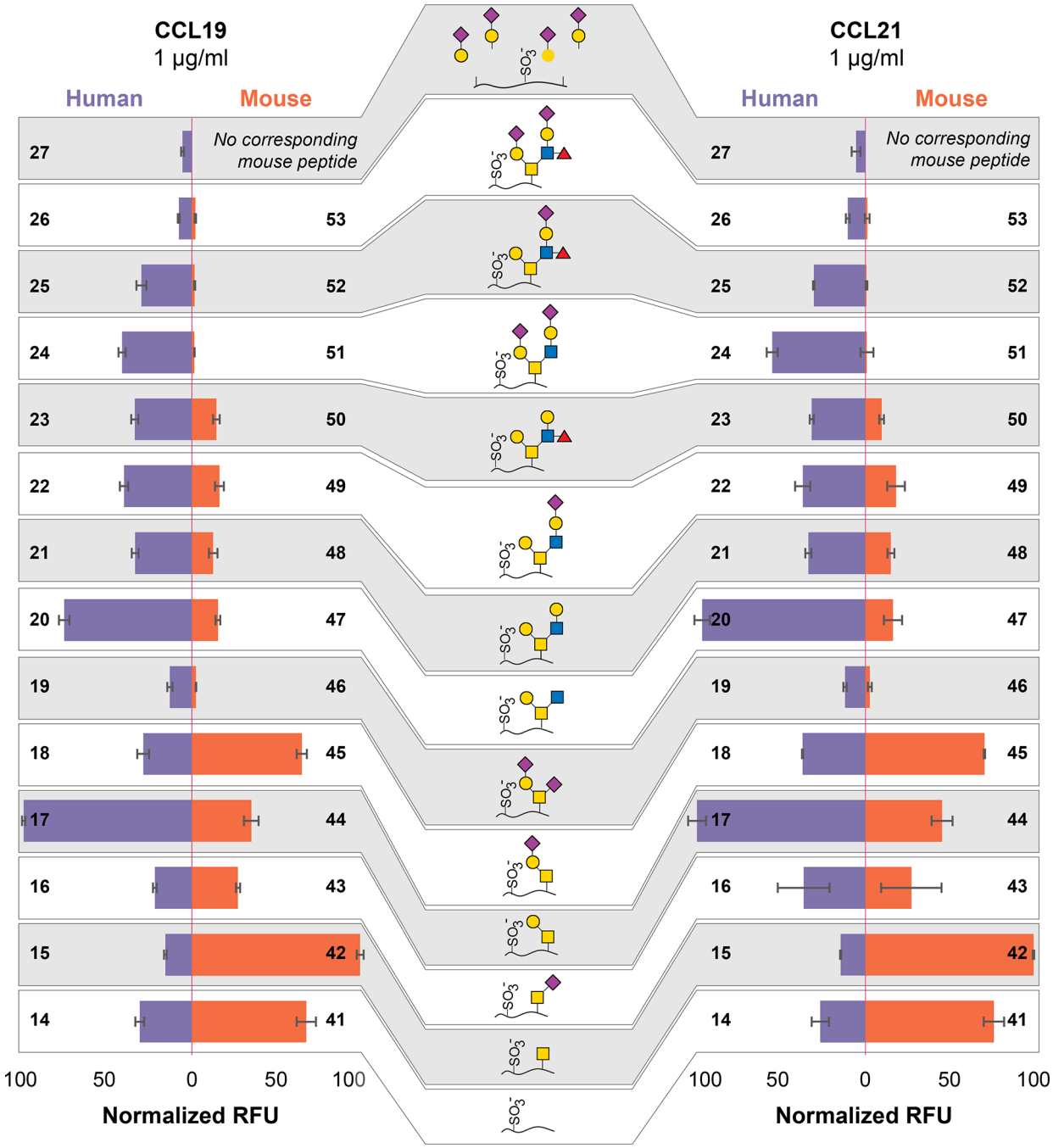

Figure 4. CCL19 and CCL21 binding to the glycosulfopeptide PSGL-1 microarray

Comparison of CCL19 (left) and CCL21 (right) binding to human and mouse PSGL-1 sulfated peptides. The microarray was probed with CCL19 and CCL21 to investigate the effect of different glycan structures and sulfation status for binding. CCL19 and CCL21 showed very similar binding with tyrosine sulfation being pivotal for binding, whereas 2 X SLe^x (**27**) and di-sialyl-Le^x (**26**) almost completely abolished the binding of both CCL19 and CCL21 to human PSGL-1. In the mouse sequences, less complex structures such as di-sialyl T (**53**) and sialylated branch core 2 structures (**38** and **39**) blocked the CCL19 and

CCL21 binding. Full microarray data available in Figure S3. Y-axis = relative fluorescent units (RFU), error bars = +/− 1 standard deviation.

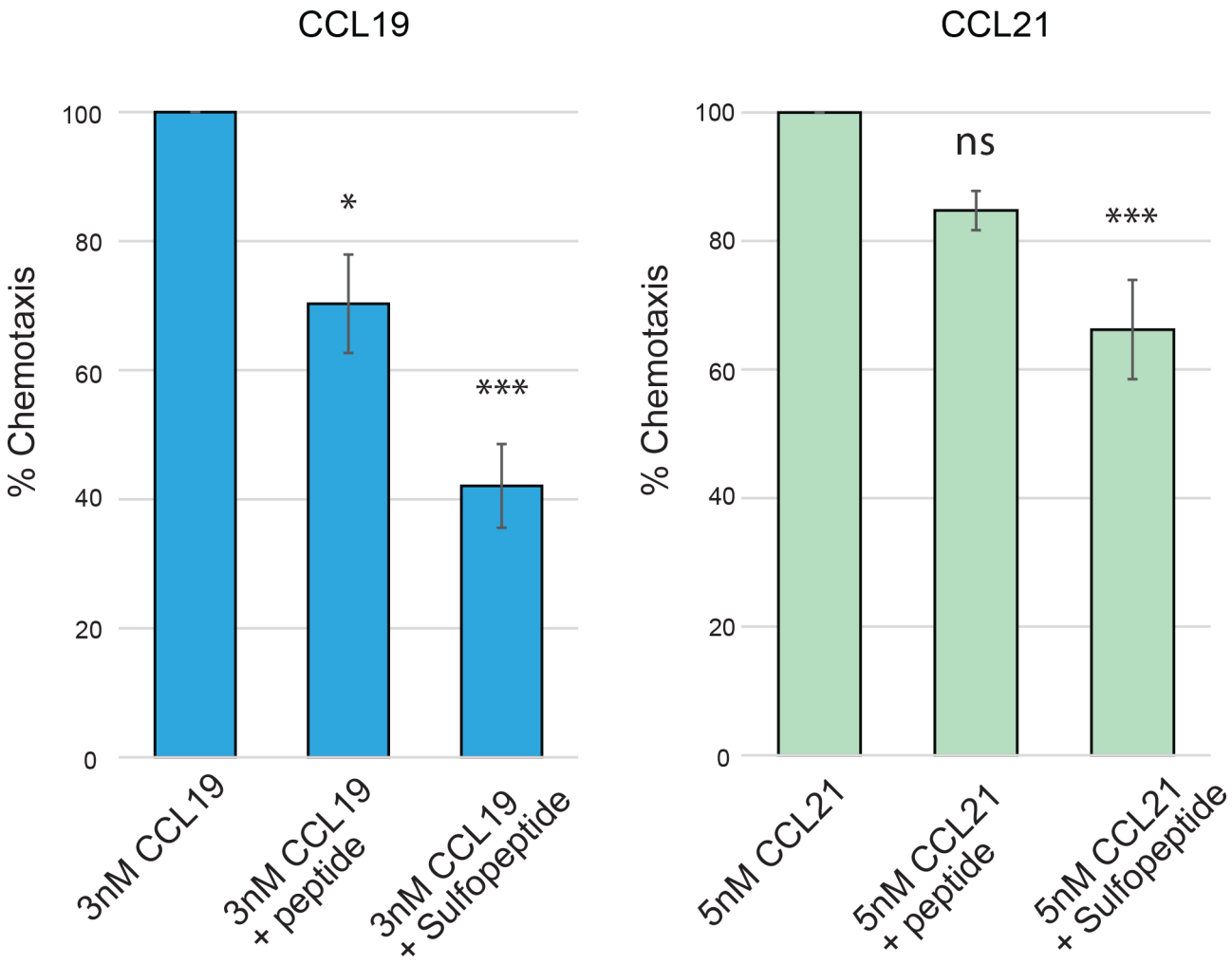

Figure 5. PSGL-1 sulfopeptide inhibits chemotaxis of primary human dendritic cells

Chemotaxis by primary human dendritic cells towards CCL19 and CCL21 measured using transwell inserts. Migration without any PSGL-1 peptide added was set to 100% and compared to migration with hPSGL-1 sulfopeptide (**14**) or unmodified peptide (**1**). Incubation with sulfopeptide shows clear reduction of the chemotactic index for both CCL19 and CCL21. Unmodified peptide also inhibited chemotaxis towards CCL19, to a smaller degree than the sulfated peptide, ns = not significant; * = $P \leq 0.05$, *** = $P \leq 0.001$. 2 biological replicates with 2 technical replicates.

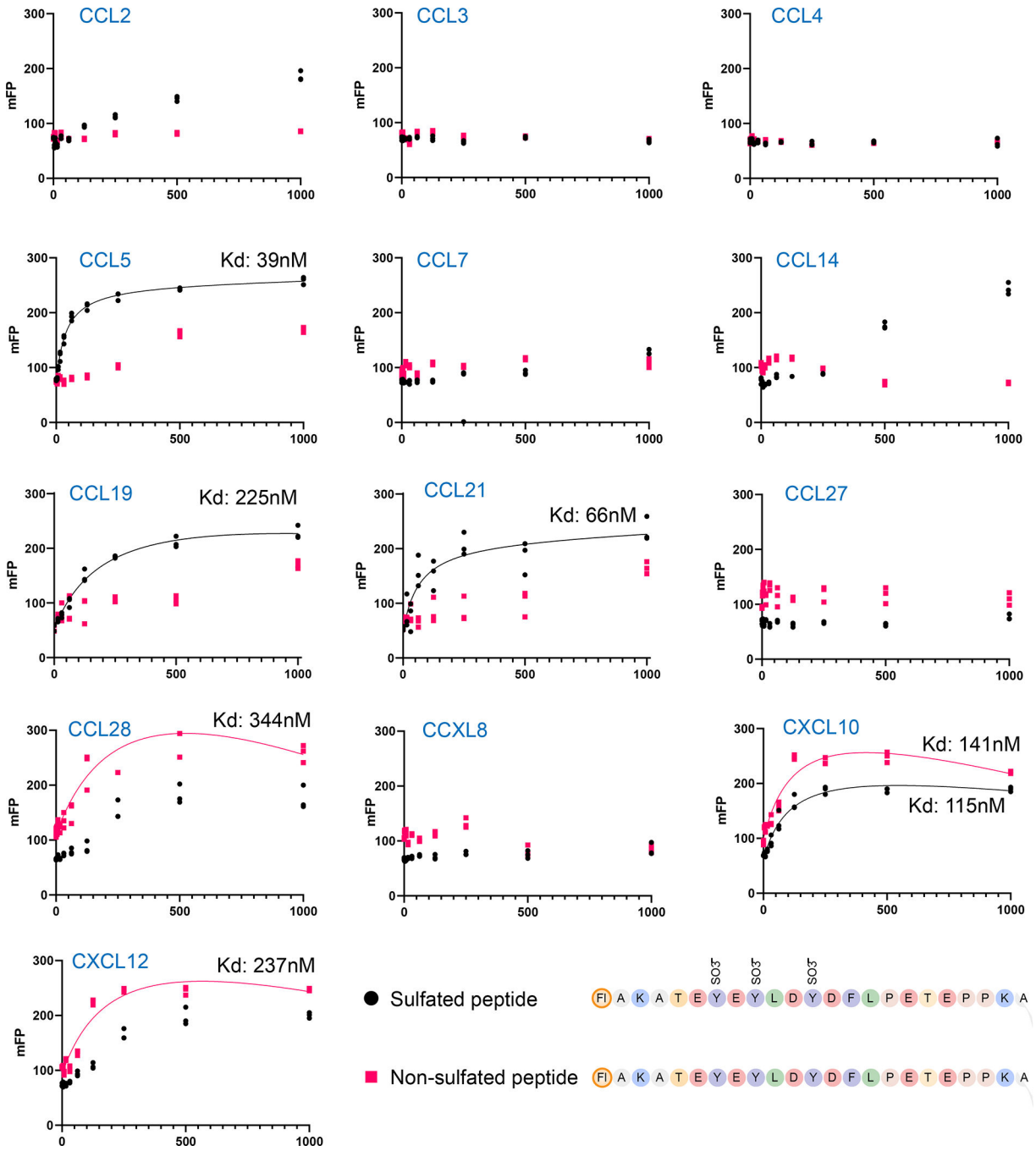

Figure 6. Fluorescence polarization assay reveals novel chemokine ligands for PSGL-1

Fluorescence polarization assay using sulfated (black circle) and naked non-sulfated (red square) human PSGL-1 peptides and chemokines were performed. The x-axis shows the nanomolar concentration of the chemokine and y-axis shows the fluorescence polarization as mFP units, Strong binding was observed for CCL5, CCL28, CXCL10, CXCL12, CCL19 and CCL21; no binding was observed for CCL2, CCL3, CCL4, CCL7, CCL14, CCL27

and CXCL8. K_d shown above individual graphs. K_d calculated using Microsoft Excel and GraphPad Prism by a non-linear fit. Peptide sequences are shown in lower right.

KEY RESOURCES TABLE

REAGENT or RESOURCE	SOURCE	IDENTIFIER
Antibodies		
Anti-sTyr Anti-Sulfotyrosine Antibody, Clone Sulfo-1C-A2	Millipore	Cat# 05-1100 RRID:AB_1163515
Human CCL21/6Ckine Antibody	R&D systems	Cat# AF366 RRID:AB_355327
Human CCL19/MIP-3 beta Antibody	R&D systems	Cat# AF361, RRID: AB_355323
Mouse anti-Human CCL5/RANTES	R&D systems	Cat#MAB278 RRID: AB_358196
KPL-1	Santa Cruz	Cat# sc-13535, RRID:AB_626929
Goat anti-Mouse IgG (H+L), Alexa Fluor 633	Thermo Fisher	Cat# A-21052, RRID:AB_2535719
Goat anti-Mouse IgM Heavy Chain Cross-Adsorbed, Alexa Fluor 633	Thermo Fisher	A-21046, RRID:AB_2535715
Goat anti-Human IgG (H+L), Alexa Fluor 647	Thermo Fisher	Cat# A-21091, RRID:AB_2535747
Chemicals, Peptides, and Recombinant Proteins		
Whatman® quantitative filter paper, hardened low-ash, Grade 50	Sigma Aldrich	Cat# WHA1450916
1-Methyl-2-pyrrolidinone (NMP) biotech grade, >99.7%	Sigma Aldrich	Cat#494496-1L
1-Hydroxybenzotriazole hydrate (HOBt) wetted with not less than 14 wt. % water, 97%	Sigma Aldrich	Cat#157260-100G
Bromophenol blue	Sigma Aldrich	Cat#114391-5G
Anhydrous amine-free N,N-Dimethylformamide (DMF)	VWR	Cat#AA43465-K7
N,N'-Diisopropylcarbodiimide (DIC) 99%, AcroSeal™	ACROS Organics	Cat#AC446181000
Fmoc-Thr(α-D-GalNAc(Ac)3)-OH	Sussex Research	Cat#GA131000
Fmoc-Thr(Galβ(1–3)GalNAc)-OH, peracetate	Sussex Research	Cat#GA131010
Fmoc-Thr(Galβ(1–3)(GlcNAcβ(1–6))GalNAc-OH, Peracetate	Sussex Research	GA131030
Fmoc-Tyr(SO3nP)-OH	Bacchem	4082682
5(6)-Carboxyfluorescein, (5,6)-FAM	Sigma	8510820005
UDP-GalNAc	Chemily	SN02010
UDP-Galactose	Carbosynth	MU06699
CMP-sialic acid	Chemily	SN02001
GDP-Fucose	Chemily	SN02002
Biotinylated *Vicia villosa* Lectin (VVL)	Vector Labs	Cat#B-1235-2
Biotinylated *Aleuria aurantia* Lectin (AAL)	Vector Labs	B-1395-1
Recombinant Human E-Selectin/CD62E Fc Chimera Protein, CF	R&D systems	724-ES
Recombinant Mouse P-Selectin/CD62P Fc Chimera Protein	R&D systems	737-PS
Recombinant Human P-Selectin/CD62P Protein	R&D systems	ADP3
Recombinant Human PSGL-1/CD162 Fc Chimera Protein, CF	R&D systems	3345-PS-050
PNGase F	New England Biolabs (NEB)	P0704L
Sequencing Grade Modified Trypsin	Promega	V5111
Endoproteinase Asp-N from *Pseudomonas fragi* mutant strain	Sigma-Aldrich	P3303-1VL
T-Synthase	Richard Cummings [53,54]	N/A

REAGENT or RESOURCE	SOURCE	IDENTIFIER
Cosmc	Richard Cummings [53,54]	N/A
Il-2	Peprotech	200–02
GM-CSF	Peprotech	300–03
X-VIVO™ 1	Lonza	BE02-060Q
Neuraminidase	Roche	10269611001
β1–4 galactosidase	NEB	P0745L
β1–3 galactosidase	NEB	P0726S
CCL2	Chemotactics	CCL2-50ug
CCL3	Chemotactics	CCL3-50ug
CCL4	Chemotactics	CCL4-50ug
CCL5	Chemotactics R&D Systems	CCL5-50ug 278-RN-050/CF
CCL7	Chemotactics	CCL7-50ug
CCL14	Chemotactics	CCL14-50ug
CCL27	Chemotactics	CCL27-50ug
CCL28	Chemotactics	CCL28-50ug
CXCL8	Chemotactics	CXCL8-50ug
CXCL10	Chemotactics	CXCL10-50ug
CXCL12	Chemotactics	CXCL12-50ug
CCL19	R&D Systems Chemotactics	361-MI-025/CF CCL19-50ug
CCL21	R&D Systems	366-6C-025/CF
Critical Commercial Assays		
CellTiter glo	Promega	G7570
Deposited data		
LC-MS data deposited in PRIDE	This Paper	PXD042685
Data for all figures and MALDI spectra deposited in Harvard Dataverse	This Paper	https://doi.org/10.7910/DVN/V7T98V
Recombinant DNA		
Plasmid: ST6GalNAc1-pGEn2	Kelley Moremen [55]	N/A
Plasmid: GCNT1-pGEn2	Kelley Moremen	HsCD00413067
Plasmid: FUT6-pGEn2	Kelley Moremen [55]	N/A
Plasmid: B1,4GalT	Kelley Moremen [55]	N/A
Plasmid: ST3Gal4	Kelley Moremen [55]	N/A
Plasmid: ST3Gal1	Kelley Moremen [55]	N/A
Software and Algorithms		
Excel	Microsoft	N/A
Prism	GraphPad	N/A
Origin	OriginLab	N/A
Byonic™	Protein Metrics	N/A

REAGENT or RESOURCE	SOURCE	IDENTIFIER
Other		
Snap-lock type glass food container	Target	N/A
Reusable biopsy punch (0.5mm tip)	World Precision Instruments	Cat#504639
Nexterion® Slide H 3D NHS (Schott) slides	Applied Microarrays	Cat#1070936
Corning® Transwell® polycarbonate membrane cell culture inserts	Merck	CLS3421